bioRxiv preprint doi: https://doi.org/10.1101/809541; this version posted October 18, 2019. The copyright holder for this preprint (which was not certified by peer review) is the author/funder. All rights reserved. No reuse allowed without permission.

Large DNA virus promoted the endosymbiotic evolution to make a photosynthetic eukaryote

Authors and Affiliations

Mitsuhiro Matsuo[1], Atsushi Katahata[1], Makoto Tachikawa[1], Yohei Minakuchi[2], Hideki Noguchi[3,4], Atsushi Toyoda[2,4], Asao Fujiyama[4], Yutaka Suzuki[5], Takayuki Hata[1], Soichirou Satoh[1], Takuro Nakayama[6,7], Ryoma Kamikawa[8], Mami Nomura[8,9], Yuji Inagaki[6], Ken-ichiro Ishida[9], Junichi Obokata[1]

[1]Graduate School of Life and Environmental Science, Kyoto Prefectural University, Kyoto, 606-8522, Japan.

[2]Department of Genetics and Evolutionary Biology, National Institute of Genetics, Mishima, Shizuoka, 411-8540, Japan.

[3]Center for Genome Informatics, Joint Support-Center for Data Science Research, Research Organization of Information and Systems, Mishima, Shizuoka 411-8540, Japan.

bioRxiv preprint doi: https://doi.org/10.1101/809541; this version posted October 18, 2019. The copyright holder for this preprint (which was not certified by peer review) is the author/funder. All rights reserved. No reuse allowed without permission.

[4]Advanced Genomics Center, National Institute of Genetics, Mishima, Shizuoka 411-8540, Japan.

[5]Graduate school of Frontier Science, University of Tokyo, Kashiwa, Chiba, 272-8562, Japan.

[6]Center for Computational Sciences, University of Tsukuba, Tsukuba, Ibaraki, 305-8577, Japan.

[7]Graduate School of Life Sciences, Tohoku University, Sendai 980-8578, Japan

[8]Graduate Schools Human and Environmental Studies, Kyoto University, Kyoto, 606-8501, Japan.

[9]Graduate School of Life and Environmental Sciences, University of Tsukuba, Tsukuba, Ibaraki, 305-8572, Japan.

bioRxiv preprint doi: https://doi.org/10.1101/809541; this version posted October 18, 2019. The copyright holder for this preprint (which was not certified by peer review) is the author/funder. All rights reserved. No reuse allowed without permission.

Abstract

Chloroplasts in photosynthetic eukaryotes originated from a cyanobacterial endosymbiosis far more than 1 billion years ago[1-3]. Due to this ancientness, it remains unclear how this evolutionary process proceeded. To unveil this mystery, we analysed the whole genome sequence of a photosynthetic rhizarian amoeba[4], *Paulinella micropora*[5,6], which has a chloroplast-like organelle that originated from another cyanobacterial endosymbiosis[7-10] about 0.1 billion years ago[11]. Here we show that the predacious amoeba that engulfed cyanobacteria evolved into a photosynthetic organism very quickly in the evolutionary time scale, probably aided by the drastic genome reorganization activated by large DNA virus. In the endosymbiotic evolution of eukaryotic cells, gene transfer from the endosymbiont genome to the host nucleus is essential for the evolving host cell to control the endosymbiont-derived organelle[12]. In *P. micropora*, we found that the gene transfer from the free-living and endosymbiotic bacteria to the amoeba nucleus was rapidly activated but both simultaneously ceased within the initiation period of the endosymbiotic evolution, suggesting that the genome reorganization drastically proceeded and completed. During this period, large DNA

bioRxiv preprint doi: https://doi.org/10.1101/809541; this version posted October 18, 2019. The copyright holder for this preprint (which was not certified by peer review) is the author/funder. All rights reserved. No reuse allowed without permission.

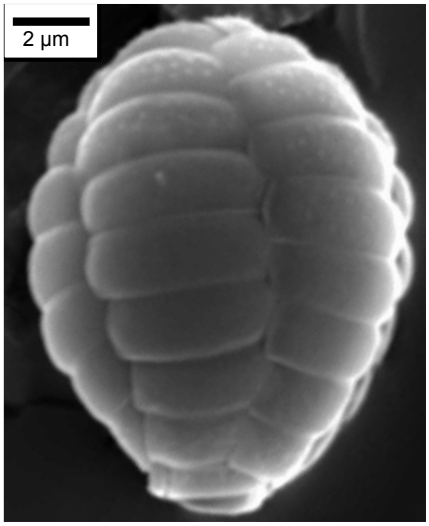
virus appeared to have infected the amoeba, followed by the rapid amplification and diversification of virus-related genes. These findings led us to re-examine the conventional endosymbiotic evolutionary scenario that exclusively deals with the host and the symbiont, and to extend it by incorporating a third critical player, large DNA virus, which activates the drastic gene transfer and genome reorganization between them. This *Paulinella* version of the evolutionary hypothesis deserves further testing of its generality in evolutionary systems and could shed light on the unknown roles of large DNA viruses[13] in the evolution of terrestrial life.

Main manuscript

Our laboratory culture of *P. micropora* MYN1[5,6] (Fig. 1a) is not axenic and contains bacteria. From this culture, we prepared the chromatins of *P. micropora* by micromesh-aided cell isolation and chromatin immunoprecipitation using a canonical histone antibody. Shotgun sequencing of this chromatin DNA gave us a high-quality draft genome assembly of 967 Mb (Fig. 1, Extended Data Fig. 1, Supplementary Table 1). K-mer analysis estimated the genome size of *P. micropora* MYN1 to be 1.35 Gb

bioRxiv preprint doi: https://doi.org/10.1101/809541; this version posted October 18, 2019. The copyright holder for this preprint (which was not certified by peer review) is the author/funder. All rights reserved. No reuse allowed without permission.

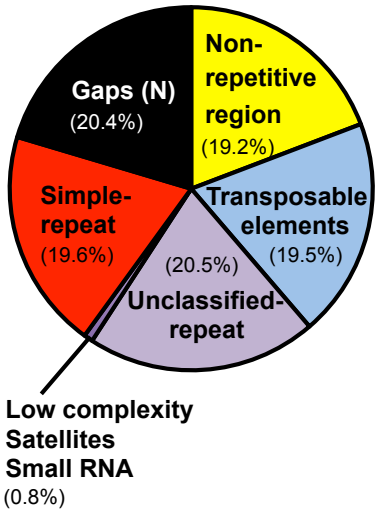
a



b

Total Scaffold length	966,816,691 bp
Scaffolds No.	8,276
Scaffold N50	468,729 bp
%GC	44.01
Gene No.	36,763
Average Gene size (cds size)	10,400 bp (1,522 bp)
Average intron No. per gene	7.9

c



d

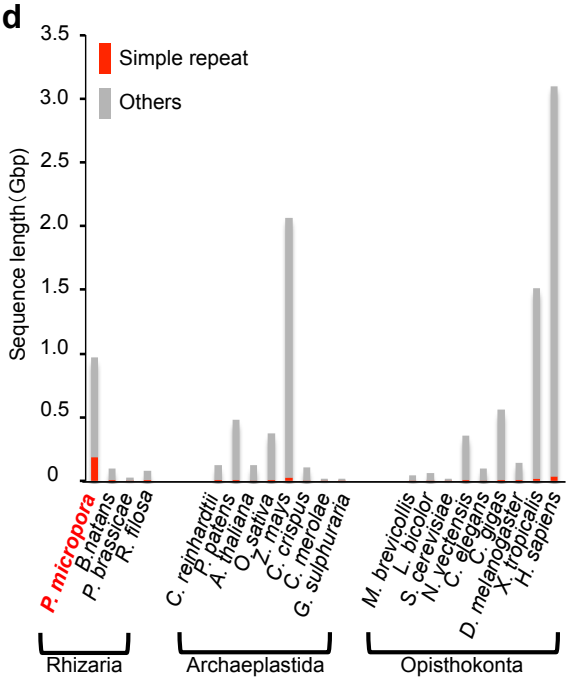


Fig. 1. An overview of the *P. micropora* MYN1 draft genome. a, A SEM image of *P. micropora* MYN1. **b,** The statistics of the draft genome. **c,** The genome composition of *P. micropora* MYN1 analysed by RepeatMasker[27]. **d,** Simple repeats are extraordinarily rich in *P. micropora* MYN1 compared with other organisms.

bioRxiv preprint doi: https://doi.org/10.1101/809541; this version posted October 18, 2019. The copyright holder for this preprint (which was not certified by peer review) is the author/funder. All rights reserved. No reuse allowed without permission.

(Extended Data Fig. 1); hence, our draft assembly covered 72% of the whole genome. The genome is largely composed of repeated sequences, with 19.2% unique sequences (Fig. 1c). Simple repeat sequences are extraordinarily rich, amounting to 19.6% (Fig. 1c, 1d). As much as simple repeats and transposons, 20.5% of the genome is occupied by unclassified repeat sequences that contain notable amounts of DNA virus-like fragments (Fig. 1c, Supplementary Table 2, 3).

A total of 36,763 protein gene models were predicted; on average, they were 10.4 kb long and contained eight introns, implying large and complex structures (Fig. 1b, Supplementary Table 4). Their gene ontology (GO) term analysis showed that DNA-related metabolism which associated with DNA virus is significantly over-represented compared with that of other rhizarian organisms (Extended Data Fig. 1e, Supplementary Table 5).

From the above gene set of *P. micropora*, we attempted to characterize the genes that have been pivotal for the endosymbiotic evolution. We extracted the genes derived from cyanobacteria as well as those derived from the rest of the bacteria; we refer to the former as endosymbiotic gene transfer (EGT) candidates and the latter as

bioRxiv preprint doi: https://doi.org/10.1101/809541; this version posted October 18, 2019. The copyright holder for this preprint (which was not certified by peer review) is the author/funder. All rights reserved. No reuse allowed without permission.

82 horizontal gene transfer (HGT) candidates in this study. We obtained 177 EGT and 248
83 HGT candidates (Fig. 2, Supplementary Table 6). Half of the EGT candidates are genes
84 for high light inducible proteins (HLIPs)[12], which are involved in the protection against
85 excess light energy. Phylogenetic analysis of these HLIPs showed that they are
86 polyphyletic, suggesting that HLIPs should have been acquired by multiple independent
87 gene transfers from cyanobacteria (Extended Data Fig. 2). Thus, the gain of a light
88 protection system should have been crucial for the predacious amoeba to evolve into a
89 photosynthetic organism.

90 HGT candidates contain genes of diverse functions, including ribosome
91 biogenesis, DNA synthesis and amino acid metabolism. These genes appear to be
92 involved in (1) endosymbiont biogenesis and (2) changes of the cellular nutrient state
93 from heterotrophy to photo-autotrophy. To further examine the genes essential to the
94 evolution of a photosynthetic organism, we compared orthologs among *P. micropora*,
95 primary photosynthetic eukaryotes and predaceous eukaryotes (Extended Data Fig. 3a,
96 3b); 12 orthologous groups are conserved in the former two but not in the latter,
97 including the genes for light acclimation, organelle gene expression and changes of the

bioRxiv preprint doi: https://doi.org/10.1101/809541; this version posted October 18, 2019. The copyright holder for this preprint (which was not certified by peer review) is the author/funder. All rights reserved. No reuse allowed without permission.

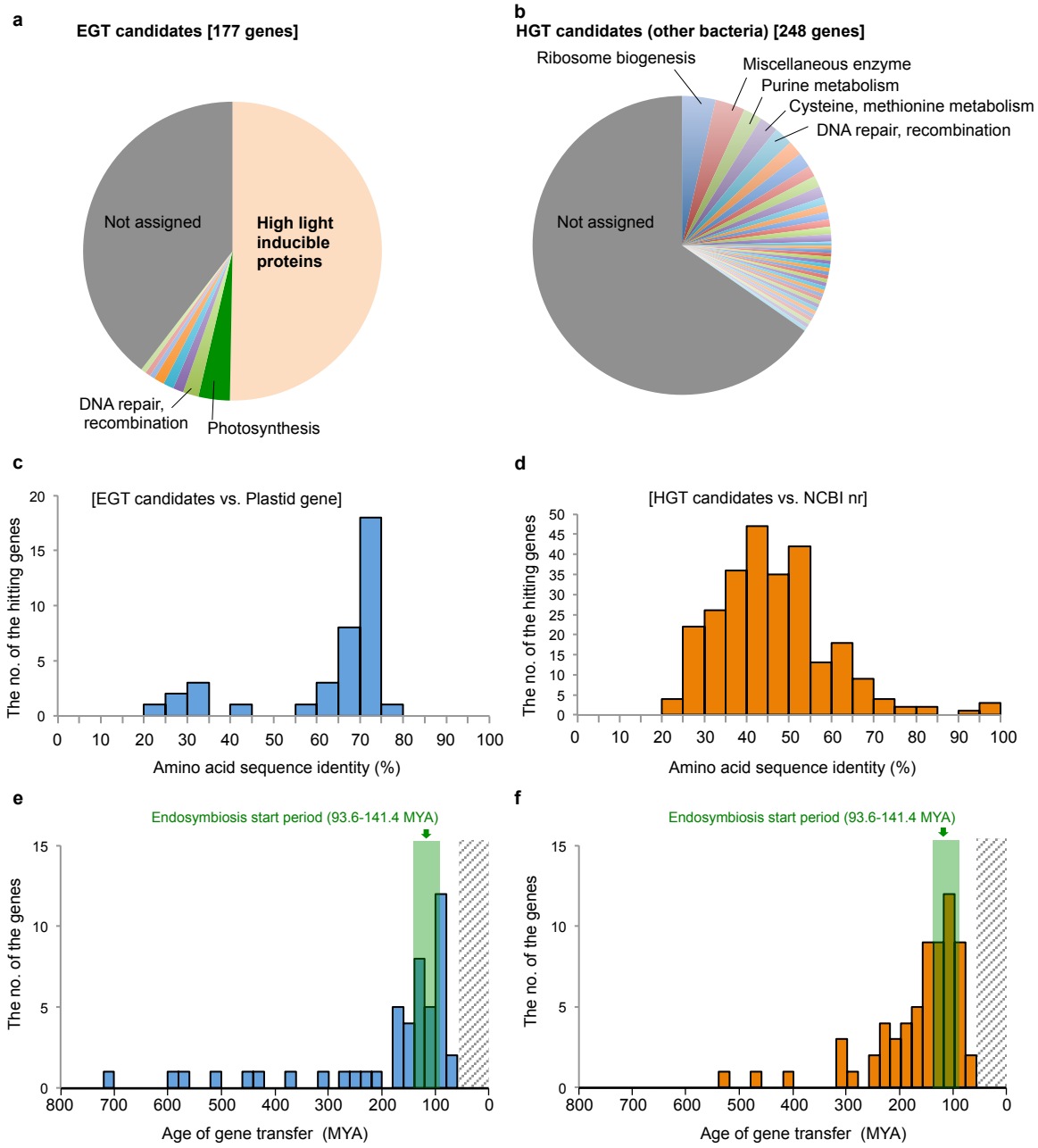


Fig. 2. *P. micropora* nuclear genes acquired by EGT/HGT. a, b, A functional classification of the *P. micropora* nuclear genes derived from cyanobacteria (EGT candidates) (**a**), and those from other bacteria (HGT candidates) (**b**). **c, d,** The amino acid sequence identity of EGT candidates against *P. micropora* MYN1 plastid genes (**c**) and that of HGT candidates against bacterial genes of the NCBI nr database (**d**). **e, f,** An estimation of the gene transfer age for EGT candidates (**e**) and HGT candidates (**f**). The endosymbiosis initiation period is green-highlighted. The ages of gene transfer in (**e**) and (**f**) were calculated based on the divergent time points (45.7–64.7 MYA) of two *Paulinella* species; thus, a gene transfer age younger than 60 MYA (striped phase) could not be estimated.

bioRxiv preprint doi: https://doi.org/10.1101/809541; this version posted October 18, 2019. The copyright holder for this preprint (which was not certified by peer review) is the author/funder. All rights reserved. No reuse allowed without permission.

98 cellular nutrient state. Some of them were obtained horizontally from eukaryotes
99 (Extended Data Figs. 3b–d). Therefore, *P. micropora* utilized the genes of diverse
100 origins for endosymbiotic evolution.

101 The biggest challenge of this study is to elucidate the temporal sequence of
102 the events that occurred at the birth of photosynthetic eukaryotes. To solve this puzzle,
103 we first estimated how and when EGT occurred, based upon the sequence similarity
104 between the EGT candidates and organelle-encoded genes. The results were surprising.
105 We could not find any case with more than 80% amino acid sequence identity
106 conserved between them (Fig. 2c), suggesting that plastidial EGT did not occur in a
107 recent time period (Fig. 2e). We further searched for nuclear-localized plastid DNAs
108 and nuclear-localized mitochondria DNAs[15,16] in the genome and found the latter but
109 not the former. Therefore, it is likely that plastidial EGT rapidly activated and then
110 ceased early in the endosymbiotic evolution in *P. micropora*, while this cool down was
111 not found for mitochondrial EGT (Extended Data Fig. 4).

112 We confirmed this hypothesis from the different angle. Phylogenetic tree
113 analysis of the EGT candidates showed that most of them already lost their counterparts

bioRxiv preprint doi: https://doi.org/10.1101/809541; this version posted October 18, 2019. The copyright holder for this preprint (which was not certified by peer review) is the author/funder. All rights reserved. No reuse allowed without permission.

in the plastid genome, except for four genes; hence, we reckon that these four genes were transferred from the plastid to the nucleus relatively recently. The divergences of the four genes between their nuclear and plastid counterparts were estimated to have occurred 319.8 to 98.6 million years ago (MYA) (Extended Data Fig. 5). Considering that the photosynthetic *Paulinella* species have diverged from the heterotrophic species 141.4 to 93.6 MYA[11], even the latest EGT at 98.6 MYA had occurred within the initiation period of the endosymbiotic evolution. Taken together, the results of this study strongly suggest that EGT rapidly activated and ceased within the initial period of the endosymbiotic evolution (Fig. 2e), and a similar time course was also found for HGT (Fig. 2d, 2f).

What does this rapid and simultaneous cool-down of EGT and HGT (Figs. 2c–2f) mean? The most simple and likely explanation is that the predaceous *Paulinella* shrank and lost phagocytic activity at this time to become a photosynthetic organism, accompanied by the shut-down of phagocytosis-aided EGT/HGT. In reality, HGT from prey cyanobacteria occurred in the predaceous *Paulinella* species[17]. If our assumption is correct, the predaceous *Paulinella* should have changed its cellular, genomic and

bioRxiv preprint doi: https://doi.org/10.1101/809541; this version posted October 18, 2019. The copyright holder for this preprint (which was not certified by peer review) is the author/funder. All rights reserved. No reuse allowed without permission.

130 metabolic systems very quickly in terms of the evolutionary time scale. How was this
131 drastic change possible? To examine this, we re-focused this study on DNA virus-like
132 fragments frequently found in the *P. micropora* genome.

133 Fig. 3a shows a genomic scaffold containing putative virus fragments that are
134 characterized by having from a dozen to a hundred copies, high GC content, ORFs
135 similar to eukaryotic virus genes, and many intron-less genes of heterogeneous origins
136 with unknown functions (Extended Data Fig. 6, Supplementary Table 3). In addition,
137 they are often intermingled with simple repeats and mobile genetic elements, i.e.,
138 Maverick/Polinton-type giant transposons[18,19] and retrotransposons. Most notably, the
139 maximum fragment size reaches 300 kb (Extended Data Fig. 6). These structural
140 features of the DNA virus-like fragments resemble those of nucleocytoplasmic large
141 DNA viruses (NCLDV)[20] whose genome size ranges from 100 kbp to 2.5 Mbp and who
142 have many genes of heterogenous origins with unknown functions. However, a
143 phylogenetic analysis based on DNA polymerases shows that those genes, encoded by
144 the putative viral fragments, form a monophyletic clade distant from the genes of
145 eukaryotes, prokaryotes and known NCLDVs (Fig. 3b). Therefore, we assume that they

bioRxiv preprint doi: https://doi.org/10.1101/809541; this version posted October 18, 2019. The copyright holder for this preprint (which was not certified by peer review) is the author/funder. All rights reserved. No reuse allowed without permission.

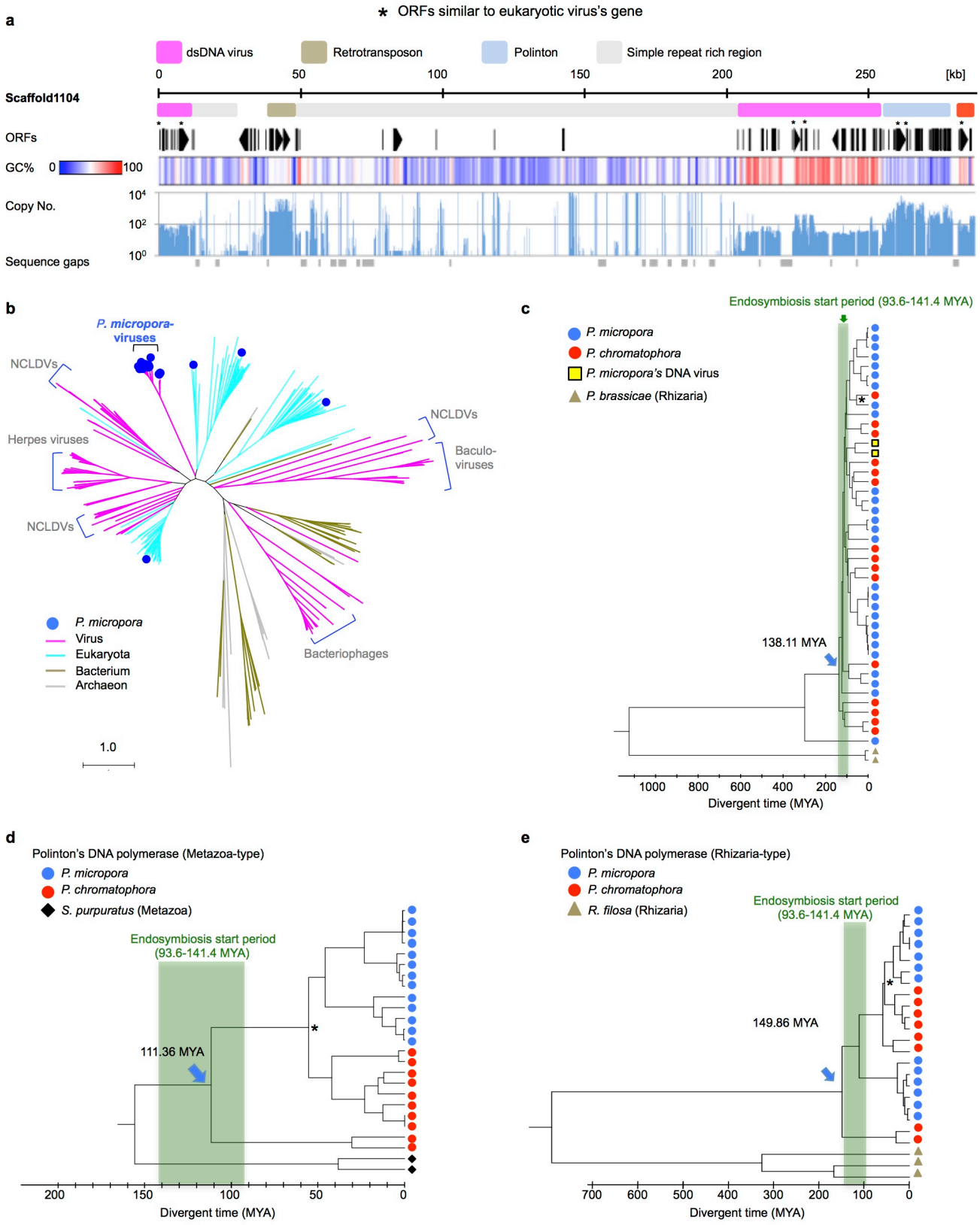


Fig. 3. Putative DNA virus and mobile elements in *P. micropora* MYN1. a, A schematic view of DNA virus-like fragments and mobile elements in the *P. micropora* draft genome (Scaffold 1104). The genomic regions were coloured according to the sequence characteristics; putative dsDNA virus (pink), Polinton (light blue), retrotransposon (brass yellow) and simple repeat-rich region (grey). The copy number of the interspersed repeat elements was analysed by BLASTN against the simple-repeat-masked *P. micropora* draft genome. **b,** ML phylogenetic tree of DNA polymerases of viruses, eukaryotes and prokaryotes. **c,** Divergent time analysis of the virus-type GPCR in *Paulinella*'s lineage. **d, e,** Divergent time analysis of DNA polymerase genes of metazoa-type (**d**) and rhizarian-type (**e**) Polintons. Asterisks: the branch point of *P. micropora* and *P. chromatophora* set at 45.7–64.7 MYA. Green bands: initiation periods of endosymbiosis with cyanobacteria (93.6–141.4 MYA). *P. micropora*; *Paulinella micropora* MYN1, *P. chromatophora*; *Paulinella chromatophora* CCAC0185, *P. brassicae*; *Plasmodiophora brassicae*, *R. filosa*; *Reticulomyxa filosa*, *S. purpurgus*; *Strongylocentrotus purpuratus*.

bioRxiv preprint doi: https://doi.org/10.1101/809541; this version posted October 18, 2019. The copyright holder for this preprint (which was not certified by peer review) is the author/funder. All rights reserved. No reuse allowed without permission.

146 are from a novel large DNA virus but share several properties with known NCLDVs.

147 Our next question was when the putative virus infected the *Paulinella* lineage.
148 Although ancient infection hallmarks were already smeared, we found a suggestive case
149 in a *Paulinella*-specific gene family (Fig. 3c, Extended Data Fig. 7). The G-protein
150 coupled receptor (GPCR) genes rapidly expanded and diversified within a short
151 evolutionary period around the endosymbiosis initiation point. Noteworthily, two genes
152 of this family were found only in the putative viral fragment regions (yellow squares in
153 Fig. 3c and Extended Data Fig. 7). This suggests that these two genes diverged from the
154 rest of the family around the endosymbiosis initiation point and have been inherited
155 from the virus genome. This indicates that the putative virus has infected the *Paulinella*
156 lineage around the endosymbiosis initiation point or earlier.

157 To further prove this, we investigated the Maverick/Polinton-type transposons
158 derived from a virophage[21], which parasitizes giant viruses (extremely large NCLDVs)
159 with its propagation depending on the host virus[21,22]. Virophages are also integrated into
160 the nuclear genome and could function as an anti-DNA virus system to protect
161 eukaryotic cells from the DNA virus[23,24]. Therefore, we hypothesized that the

bioRxiv preprint doi: https://doi.org/10.1101/809541; this version posted October 18, 2019. The copyright holder for this preprint (which was not certified by peer review) is the author/funder. All rights reserved. No reuse allowed without permission.

162 emergence of Mavericks/Polintons and their amplifications have occurred concomitant
163 with the DNA virus infection. In the *P. micropora* genome, two distinct
164 Mavericks/Polintons, metazoan- and rhizaria-type, were detected in abundance
165 (Extended Data Fig. 8, Supplementary Table 7). The divergent time analysis showed
166 that both started amplification in the endosymbiosis initiation period (Fig. 3d, 3e).
167 These results of the Maverick/Polinton-type transposons support the hypothesis that the
168 large DNA virus infected the *Paulinella* lineage around the endosymbiosis initiation
169 period.

170 Recent studies of NCLDV and giant DNA virus have drastically changed our
171 conventional view of viruses[13], especially their huge potential to incorporate diverse
172 genetic materials of heterogenous origins[25,26] and to mediate their shuffling.
173 Considering these properties of large DNA virus and the results of this study, we could
174 reconstruct the initial evolutionary process of the photosynthetic *Paulinella* species as
175 shown in Fig. 4. In this hypothetical model, large DNA virus contributed to the
176 endosymbiotic evolution as a critical player, in addition to the original players of the
177 host and symbiont. We should note that, in general, the detection of ancient infection

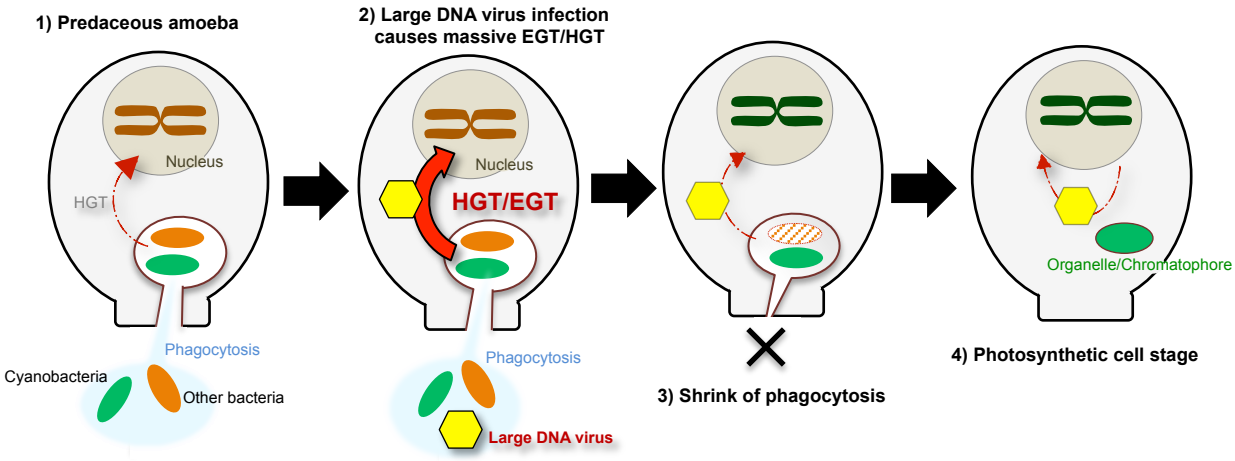


Fig. 4. Initial process of the endosymbiotic evolution of photosynthetic *Paulinella* species modeled from the *P. micropora* genomic data. 1) Predacious ancestors digested prey bacteria via phagocytosis with continuing low levels of HGT. **2)** The infection of large DNA virus triggered the massive HGT/EGT to promote the rapid endosymbiotic evolution. **3)** Acquiring photosynthetic competency shrunk the phagocytic activity to shut down the source of HGT/EGT. **4)** The photo-autotrophic *Paulinella* sp. contains one photosynthetic organelle per cell, hence, release of the organelle DNA hardly occurred without losing photosynthetic activity. In this final stage, virus-mediated gene transfer continued at trace level.

178 hallmarks of large DNA virus seems difficult because (1) it could be easily lost due to
179 its harmful and undesirable effects on host proliferation, (2) of poor information of the
180 virus sequences and (3) of repeated sequences that are apt to be omitted in the assembly
181 process of the genomic sequencing projects. This *Paulinella* version of the
182 endosymbiotic evolution hypothesis deserves further examination to test its generality
183 in many evolutionary systems.
184
185 **Methods**
186 **Data availability**
187 The sequences of the *P. micropora* draft genome, plastid (chromatophore) genome,
188 mitochondria genome and the raw reads data set were deposited to the DDBJ
189 (Accession No. are shown in Supplemental Table 8) and DDBJ reads archives (DRA
190 Accession No. DRA003059, DRA003106, DRA008524).
191
192 ***P. micropora*** **culture and cell isolation.** The *P. micropora* MYN1 strain (NIES
193 Collection, Tsukuba, JAPAN, NIES-4060) was cultured according to Nomura et al.

194 (2014)[5] and harvested by low-speed centrifugation (500 × g, 2 min) at 4 °C. The
195 harvested cells were resuspended in the culture medium and filtrated through a 20 μm
196 mesh nylon filter (HD-20, Nippon Rikagaku Kikai Co., Ltd., Tokyo, Japan) to remove
197 dead cell aggregates with high bacterial contamination. Recovered healthy cells were
198 repeatedly washed with culture medium and subjected to RNA extraction. For
199 extraction of chromatin DNA, the cells were subsequently washed three times with 10
200 mM Tris-HCL (pH 8.0), six times with 10 mM Tris-HCL (pH 8.0) plus 10 mM EDTA,
201 and recovered by a 5 μm mesh nylon filter (PP-5n, Kyoshin Rikoh Inc., Tokyo, Japan)
202 to give clean cells largely free of bacterial contamination.
203
204 **Chromatin and genomic DNA extraction.** Genomic DNA used for paired-end (300 b,
205 500 b) and mate-pair (3 kb, 5 kb) libraries for HiSeq sequencing were purified by
206 chromatin immunoprecipitation (ChIP) as follows. Ten milligrams of *P. micropora* cells
207 were homogenized in 500 μl homogenizing buffer (20 mM Tris-HCl (pH 7.6), 10 mM
208 NaCl, 10 mM KCl, 2.5 mM EDTA, 250 mM sucrose, 0.1 mM spermine, 0.5 mM
209 spermidine and 1 mM DTT) using a 30μm clearance glass homogenizer (RD440911,

210 Teraoka Co., Ltd., Osaka, Japan). After centrifugation (1000 × g, 10 min, 4 °C), the
211 pellets were resuspended in 300 μl ChIP buffer (50 mM Tris-HCl (pH 8.0), 500 mM
212 NaCl, 10 mM EDTA, 0.1% SDS, 0.5% Na-deoxycholate, 1% Triton X-100, 1 mM DTT
213 and 10% glycerol) with 20 μl Dynabeads protein G (Thermo Fisher Scientific, MA,
214 U.S.A.) charged with 1 μg anti-histone H3 antibody (Ab1791) (Abcam plc, Cambridge,
215 UK) and incubated at 4 °C for 20 min. Dynabeads were then washed twice with ChIP
216 buffer, twice with glycerol-free ChIP buffer and finally suspended in DNA extraction
217 buffer (10 mM Tris-HCl (pH 8.0), 1 mM EDTA and 1% SDS). After RNase A (10
218 μg/ml) and proteinase K (200 μg/ml) treatment, DNAs were purified by using Plant
219 DNeasy Mini Kit (Qiagen, Hilden, Germany). For the construction of the long mate-pair
220 libraries (12 kb, 15 kb, 18 kb and 20 kb), the total *P. micropora* genome was extracted
221 without ChIP purification.
222
223 **Genome sequencing and assembly.** Sequencing libraries were prepared using a
224 TruSeq DNA PCR-Free Library Preparation Kit and a Nextera Mate Pair
225 Library Prep Kit (Illumina, San Diego, CA). Two paired-end libraries with

300 and 500bp inserts and six mate pair libraries (3kb, 5kb, 12kb, 15kb, 18kb, and 20kb) were constructed and sequenced on the Illumina HiSeq 2500 sequencers with 151 cycles per run. The nuclear draft genome was assembled by SOAPdenovo v2.04-r240[28] with a k-mer size of 121 after removing the sequence reads of the plastid (chromatophore) and mitochondria genomes, and those of two contaminating bacteria genomes. After the genome assembly, we checked for the contamination of the organelle genome and the bacteria genomes again, and we removed the contaminants from the draft genome. K-mer frequency analysis was performed by Jellyfish[29]. Genome scaffolds longer than 1 kb were analysed in this study.

RNA-seq and Iso-Seq analysis. RNAs were extracted from *P. micropora* cells at 0, 4, 8, 12, 16 and 20 hr of 14L/10D photoperiod by Trizol® reagent (Thermo Fisher Scientific), and further purified using Plant RNeasy Mini Kit (Qiagen) with RNase-free DNase I treatment (Qiagen). Samples of the above time points were equally mixed and subjected to RNA-seq analysis using Agilent Strand Specific RNA Library Preparation

242 Kit (Agilent Technologies, CA, U.S.A) and Illumina HiSeq 2500 (Illumina). The paired
243 end reads of RNA-seq were *de novo* assembled by Trinity[30] with the default setting or
244 by CLC Genomics Workbench 7.0.3 (Qiagen) using a K-mer value of 54. The RNA-seq
245 reads were mapped on the genome with Tophat[31] and assembled with Cufflinks[32] or
246 Trinity[30]. For isoform-sequencing (Iso-Seq) of full-length transcripts, cDNAs were
247 prepared from polyA+RNA using SMARTer® PCR cDNA Synthesis Kit (Takara Bio
248 Inc., Shiga, Japan). The cDNA samples were size-fractionated with the BluePippin™
249 system (Sage Science, MA, USA) and 700–1500 bp, 1500–3000 bp and 3000–6000 bp
250 fractions were analysed with a PacBio®RSII sequencer (Pacific Biosciences, CA,
251 U.S.A.). Iso-Seq-contigs were constructed using the RS_IsoSeq protocol in SMRT
252 Analysis (v2.3.0) with the parameter of estimated cDNA size. The *de novo* assembled
253 RNA-seq-contigs and Iso-Seq-contigs were mapped to the genome by BLAT[33], and
254 each contig was annotated when at least 80% of its sequence was mapped. The mapped
255 transcript data were used to make longer transcript models with PASA2 v. 2.0.2[34].
256
257 **Annotation of repeat sequences.** Repeat sequences of *P. micropora* were identified

using the RepeatModeller package (v. open-1-0-8, http://www.repeatmasker.org) and masked by RepeatMasker v. 4.0[27], using the identified-model repeat sequences and the repeat sequences of Repbase (ver. 20150807)[35] (https://www.girinst.org/repbase/). The model repeat sequences were annotated based on the sequence homology search against the NCBI nr database by BLASTX[36]. Representative Polintons and retrotransposons in Supplementary Table 3 were identified by manual inspection of the *P. micropora* draft genome aided by a sequence similarity search using BLAST software[36].

Gene annotation. Protein genes of *P. micropora* were annotated by a combination of transcriptome-based gene modelling, *ab initio* gene prediction and protein homology-based gene prediction. In the transcriptome-based gene modelling, the transcripts were masked first by RepeatMasker because many spurious repetitive sequences, which were not removed by genome-repeat-masking, were detected. We discarded the transcript models when more than 80% of the region was masked by RepeatMasker. Exceptions were made when ORFs (> 50 aa) were predicted from the unmasked region. The ORFs and coding sequences of transcripts were predicted with

274 the Transdecoder Utility of Trinity[37]. *Ab initio* gene prediction was performed by
275 Augustus[38], whose training was performed using Iso-Seq data. Since *P. micropora*
276 protein genes often contain simple repeat sequences in the exon regions, we avoided
277 masking them for the *ab initio* gene prediction. The protein homology-based gene
278 prediction was performed by Exonerate[39] after masking both the simple repeat and the
279 interspersed repeat sequences, because the homology search in the presence of simple
280 repeat sequences generated an extraordinary number of meaningless candidates (data
281 not shown). In the Exonerate analysis, we used the protein sequences that passed the
282 prescreening by BLASTX search (*P. micropora* genome vs. a local protein database
283 composed of Uniprot and 4 rhizarian organisms, *B. natans*, *P. brassicae, P.*
284 *chromatophore* and *R. filosa*). All gene models described above were combined, and the
285 best one for each gene locus was chosen according to the bit score of the BLAST search,
286 the presence/absence of transcript and ORF length. The quality of the genome assembly
287 and the annotation was assessed by BUSCO v. 1[40].
288
289 **Detection of DNA virus-like fragments.** Genomic segments with discernible

290 boundaries and distinct from the rest of the genome by the following four criteria were
291 denoted as DNA virus-like fragments or putative DNA virus fragments: 1) repeat
292 sequences detected by RepeatModeller but distinct from retrotransposons and the
293 Maverick/Polinton-type transposons, 2) higher GC content, 3) large heterogeneous
294 intron-less gene clusters and 4) ORFs similar to DNA virus proteins are encoded; DNA
295 virus genes are found within the top 100 by BLASTP search against the NCBI nr
296 database. The detailed procedure is as follows. Genomic scaffolds containing repeat
297 sequences of the unknown class[27] were subjected to ORFfinder[41], and ORFs detected
298 were annotated by BLASTP[36] search against the NCBI nr database. The GC%
299 distribution was analysed with CLC genomic workbench 7.0.3 (Qiagen).The virus copy
300 number was analysed using the BLASTN[36] program searching the simple
301 repeat-masked draft genome for virus coding sequences (Supplementary Table 3) or 100
302 b fragments generated by slicing the virus-containing scaffolds (Fig. 3, Extended Data
303 Fig. 6). BLASTN-redundant hits were manually removed.
304
305 **GO-term-, metabolism-pathway-, orthogroup- and protein-domain analysis.**

306 GO-terms were acquired by InterproScan 5[42], and the enrichment analysis was
307 performed by web-based GOstat[43] (http://gostat.wehi.edu.au/) using 27,653 GO-terms
308 of 12,007 *P. micropora* genes and 88,634 GO-terms of 39,773 genes of 4 rhizarian
309 organisms (*B. natans, P. brassicae, R. filosa* and *P.micropora,*). Metabolism-pathways
310 were analysed using KAAS of KEGG[44] (https://www.genome.jp/kegg/kaas/).
311 Orthogroup-analysis of Extended Data Fig. 3 was performed by Orthofinder[45] using a
312 local protein database (Supplementary Table 10). Protein domain information in
313 Extended Data Fig. 7 was acquired by NCBI conserved domain (CD) search
314 (https://www.ncbi.nlm.nih.gov/Structure/cdd/wrpsb.cgi)[46].
315
316 **nuclear-localized plastid DNA (nupDNA) and mitochondria DNA (numDNA)**
317 **analysis.** Using the *P. micropora* plastid genome (DDBJ Accession No. LC490351) and
318 mitochondria genome sequence (DDBJ Accession No. LC490352) for queries, nupDNA
319 and numDNA were searched for by BLASTN against the *P. micropora* draft genome
320 and the raw sequence reads of Illumina HiSeq2500. In the raw read-based nupDNA and
321 numDNA analysis, chimeric segments of the organelle-like and non-organelle

322 sequences, which represent the junction region of nuclear localized organelle DNA,
323 were surveyed. The detected reads were assembled by CodonCode Aligner (CodonCode
324 Corporation, MA, U.S.A.). The chimera artefacts due to sequencing adaptors, or
325 contaminated bacterial and mitochondria genomes, were identified by BLAST analysis
326 using the NCBI database (nt, nr) and the mitochondria genome sequence (LC490352).
327
328 **Phylogenetic analysis and the divergent time analysis.** Multiple sequence alignment
329 analyses were performed by MUSCLE[47] and MAFFT[48]. The phylogenetic trees were
330 constructed using MEGA packages (version 6[49], 7[50] and -CC[51]) and IQ-tree[52]. The
331 divergent time analysis was performed using the RelTime method[53] implemented in
332 MEGA 6. Parameters used for phylogenetic analyses are shown in Supplementary Table
333 6 and 9, respectively.
334
335 **Analysis of EGT/HGT candidates.** *P. micropora* nuclear genes derived from
336 cyanobacteria are referred to as EGT, and those derived from the rest of the bacteria are
337 defined as HGT. To screen the EGT/HGT candidates, *P. micropora* MYN1 genes were

338 used as queries for the BLASTP search against the NCBI nr database with e-value ≤
339 $1e^{-10}$, and top-hitting genes of the *Paulinella* plastid genes or prokaryotic protein
340 sequences were selected. These genes were subjected to multiple alignment analyses by
341 MUSCLE using the protein sequences of a local protein dataset in Supplementary Table
342 10 and of the best BLASTP hit sequences. The obtained data sets were subjected to a
343 neighbour joining (NJ) phylogenetic analysis (MEGA6, 7, CC) to choose *P. micropora*
344 nuclear genes that form sister groups with prokaryotes or photosynthetic eukaryotes.
345 After fine taxon re-samplings from the NCBI nr database, the NJ analysis selection was
346 conducted again. The selected genes were finally subjected to maximum likelihood
347 (ML) analysis using MEGA packages (MEGA6, 7, CC). *P. micropora* nuclear genes
348 that satisfied at least one of the following three criteria were used as EGT and HGT
349 candidates. 1) BLAST analysis of the gene gave no hint of eukaryote genes in the NCBI
350 nr database. 2) EGT and HGT are supported by ML phylogenetic analysis with a high
351 bootstrap value. We adopted a bootstrap value of 95 as threshold when phylogenetically
352 available protein alignment sequence positions were long enough (≥ 100 aa). We
353 lowered the threshold to 70 when the available sites were less than 100 aa. 3) The gene

354 is included in the clade of photosynthetic organisms. To confirm the validity of the
355 above mentioned EGT candidate selection, we also screened the EGT candidates by
356 another independent procedure. The EGT candidates obtained by these two independent
357 analyses were almost overlapping and, therefore, used for the analysis (Supplementary
358 Table 6). The alternative analysis procedure is as follows. We performed a phylogenetic
359 analysis using the software of multiple alignment (MAFFT) and ML phylogenetic
360 analysis (IQ-tree), and alignment trimming tools (trimAI[54], BMGE[55]). We selected
361 genes hitting alpha-type cyanobacteria[56,57] within the top 100 by BLAST search against
362 a custom database, which consists of the NCBI nr database supplemented with the
363 protein sequences of 14 phylogenetically informative protists (Supplemental Table 10).
364
365 **Estimation of EGT/HGT timing.** To estimate the timing of EGT/HGT, we used *P.*
366 *micropora* genes whose counter genes of *P. chromatophora* CCAC0185 were reported
367 as EGT/HGT candidates[58,59]. In addition, we restricted the analysis to *Paulinella*
368 ortholog's pairs that form a monophyletic sister group with a high bootstrap value (≥
369 70). The nearest protein sequences of HGT/EGT candidates were surveyed from NCBI

370 nr database by BLASTP analysis. Within the top 2000 sequences of BLASTP hits, the
371 phylogenetically nearest gene sequences were estimated using NJ and ML phylogenetic
372 analysis. To estimate gene transfer timing, the branching time point when *P. micropora*
373 MYN1 separated from the nearest non-rhizarian organisms in the ML phylogenetic tree
374 was calculated using the RelTime method[55]. We used an estimated value of the
375 divergence of *P. micropora* and *P. chromatophora* (45.7–64.7 MYA) based on the 18S
376 rRNA phylogenetic tree corrected by fossil information[11,60].
377
378 **Analysis of Mavericks/Polinton transposons.** *P. micropora's* Mavericks/Polintons
379 transposons were detected from the draft genome by tBLASTN using the sequence of
380 the DNA polymerase (DNA-pol) domain. Thousands of DNA polymerase ORFs,
381 predicted from the genome sequences by Transdecoder[37], were subjected to NJ
382 phylogenetic analyses. We grouped highly similar copies. Representative sequences that
383 have long ORFs and less ambiguous amino acid residues were selected from each group
384 and subjected to ML phylogenetic analysis.
385

386 **Divergent time analysis of the mobile elements.** In the divergent time analysis of
387 Marvericks/Polintons DNA polymerases, representative DNA-pol sequences of *P.*
388 *micropora* MYN1 Polintons having the traits of recent amplification (nucleotide
389 sequence identity between the copies ≥ 90%) were used. For the DNA-pol sequences of
390 *P. chromatophora* CCAC0185 Polintons, the genome sequence-reads (SRR3217293.sra,
391 SRR3217303.sra) were searched by BLASTX (e-value < $1e^{-20}$) using the sequence of *P.*
392 *micropora* MYN1 Polintons, and then, the hit-reads were assembled into contigs with
393 CLC Genomic Workbench 7.0 (Qiagen). For the analysis of virus-type GPCR genes, in
394 addition to *P. micropora* MYN1 genes and *P. micropora* putative virus genes, the
395 translated ORFs of *P. chromatophora* CCAC0185 transcripts were analysed. The GPCR
396 gene family was detected by Orthofinder[45] and BLASTP[36] search. In this analysis, the
397 genes encoding seven intact trans-membrane domain sequences, of which all seven
398 trans-membrane helices can be identified by CD search[46], were used. Furthermore,
399 several genes predicted *ab initio* by Augustus without any supporting experimental data
400 were removed from the analysis, because their gene models appeared to be artificial
401 from applying eukaryotic splicing rules to virus-like fragments. The divergent time

402 points of the mobile elements and GPCR genes were calculated by setting the nearest
403 branching point of *P. micropora* MYN1 and *P. chromatophora* CCAC0185 at 45.7–
404 64.7 MYA.
405
406 **Statistical analysis**
407 In GO-term enrichment analysis, Fisher's exact test (two tailed test) was performed and
408 the p-values corrected with false discovery rate (Benjamini) were calculated. In the
409 phylogenetic analysis, bootstrap test with ≥100 replicates was performed.
410
411 **References**
412 1
413 Yoon, H.S., Hackett, J.D., Ciniglia, C., Pinto, G. & Bhattacharya, D. (2004) A
414 molecular timeline for the origin of photosynthetic eukaryotes. *Mol. Biol. Evol.* **21**,
415 809-18, https://doi.org/10.1093/molbev/msh075 (2004).
416
417 2

418 Sánchez-Baracaldo, P., Raven, J. A., Pisani, D. & Knoll, A. H. Early photosynthetic
419 eukaryotes inhabited low-salinity habitats. *Proc. Natl. Acad. Sci. USA* **114**,
420 E7737-E7745. https://doi.org/10.1073/pnas.1620089114 (2017).
421
422 3
423 McFadden, G. I. Origin and evolution of plastids and photosynthesis in eukaryotes.
424 *CSH Perspect Biol.* **6**, a016105, https://doi.org/10.1101/cshperspect.a016105 (2014).
425
426 4
427 Burki, F. & Keeling, P. J. Rhizaria. *Curr. Biol.* **24**, R103-R107,
428 https://doi.org/10.1016/j.cub.2013.12.025 (2014).
429
430 5
431 Nomura, M., Nakayama, T. & Ishida, K. Detailed process of shell construction in the
432 photosynthetic testate amoeba Paulinella chromatophora (euglyphid, Rhizaria). *J.*
433 *Eukaryot. Microbiol.* **61**. 317-321. https://doi.org/10.1111/jeu.12102 (2014).

6 Matsuo, M. *et al.* Characterization of spliced leader trans-splicing in a photosynthetic rhizarian amoeba, Paulinella micropora, and its possible role in functional gene transfer. *PLoS One* **13**, e0200961, https://doi.org/10.1371/journal.pone.0200961 (2018).

7 Nowack, E. C., Melkonian, M. & Glöckner, G. Chromatophore genome sequence of Paulinella sheds light on acquisition of photosynthesis by eukaryotes. *Curr. Biol.* **18**, 410-418, https://doi.org/10.1016/j.cub.2008.02.051 (2008).

8 Yoon, H. S. *et al.* A single origin of the photosynthetic organelle in different Paulinella lineages. *BMC Evol. Biol.* **9**, 98, https://doi.org/10.1186/1471-2148-9-98 (2009).

9

450 Reyes-Prieto, A. *et al*. Differential gene retention in plastids of common recent origin.
451 *Mol. Biol. Evol.* **27**, 1530-1537, https://doi.org/10.1093/molbev/msq032 (2010).
452
453 10
454 Nakayama, T. & Ishida, K. Another acquisition of a primary photosynthetic organelle is
455 underway in Paulinella chromatophora. *Curr. Biol.* **19**, R284-R285,
456 https://doi.org/10.1016/j.cub.2009.02.043 (2009).
457
458 11
459 Delaye, L., Valadez-Cano, C. & Pérez-Zamorano, B. (2016) How Really Ancient Is
460 Paulinella Chromatophora? *PLOS Curr. Tree. Life.*
461 https://doi.org/10.1371/currents.tol.e68a099364bb1a1e129a17b4e06b0c6b (2016).
462
463 12
464 Martin, W. *et al.* Evolutionary analysis of Arabidopsis, cyanobacterial,and chloroplast
465 genomes reveals plastid phylogeny and thousands of cyanobacterial genes in the

466 nucleus. *Proc. Natl. Acad. Sci. USA.* **99**, 12246-12251,
467 https://doi.org/10.1073/pnas.182432999 (2002).
468
469 13
470 Koonin, E. V. & Yutin, N. Evolution of the Large Nucleocytoplasmic DNA Viruses of
471 Eukaryotes and Convergent Origins of Viral Gigantism. *Adv. Virus Res.* **103**, 167-202,
472 https://doi.org/10.1016/bs.aivir.2018.09.002 (2019).
473
474 14
475 Komenda, J. & Sobotka, R. Cyanobacterial high-light-inducible proteins--Protectors of
476 chlorophyll-protein synthesis and assembly. *Biochim. Biophys. Acta.* **1857**, 288-295,
477 https://doi.org/10.1016/j.bbabio.2015.08.011 (2016).
478
479 15
480 Matsuo, M., Ito, Y., Yamauchi, R. & Obokata, J. The rice nuclear genome continuously
481 integrates, shuffles, and eliminates the chloroplast genome to cause chloroplast-nuclear

482 DNA flux. *Plant Cell* **17**, 665-675, https://doi.org/10.1105/tpc.104.027706 (2005).

483

484 16

485 Smith, D. R., Crosby, K. & Lee, R. W. Correlation between nuclear plastid DNA
486 abundance and plastid number supports the limited transfer window hypothesis.
487 *Genome Biol. Evol.* **3**, 365-71, https://doi.org/10.1093/gbe/evr001 (2011).

488

489 17

490 Bhattacharya, D. *et al.* Single cell genome analysis supports a link between phagotrophy
491 and primary plastid endosymbiosis. *Sci Rep.* **2**, 356, https://doi.org/10.1038/srep00356
492 (2012).

493

494 18

495 Feschotte, C. & Pritham, E. J. Non-mammalian c-integrases are encoded by giant
496 transposable elements. *Trends Genet.* **21**, 551-552,
497 https://doi.org/10.1016/j.tig.2005.07.007 (2005).

19

Kapitonov, V. V. & Jurka, J. Self-synthesizing DNA transposons in eukaryotes. *Proc. Natl. Acad. Sci. USA* **103**, 4540-4545, https://doi.org/10.1073/pnas.0600833103 (2006).

20

Koonin, E. V. & Yutin, N. Multiple evolutionary origins of giant viruses. *F1000Res.* **7**, F1000 Faculty Rev-1840, https://doi.org/10.12688/f1000research.16248.1 (2018).

21

Fischer, M. G. & Suttle, C. A. A virophage at the origin of large DNA transposons. *Science* **332**, 231-234, https://doi.org/10.1126/science.1199412 (2011).

22

La Scola, B. *et al.* The virophage as a unique parasite of the giant mimivirus. *Nature* **455**, 100-104. https://doi.org/10.1038/nature07218 (2008).

23 Fischer, M. G. & Hackl, T. Host genome integration and giant virus-induced reactivation of the virophage mavirus. *Nature* **540**, 288-291. https://doi.org/10.1038/nature20593 (2016).

24 Blanc, G., Gallot-Lavallée, L. & Maumus, F. Provirophages in the Bigelowiella genome bear testimony to past encounters with giant viruses. *Proc. Natl. Acad. Sci. USA* **112**, E5318-5326, https://doi.org/10.1073/pnas.1506469112 (2015).

25 Boyer, M. *et al*. Giant Marseillevirus highlights the role of amoebae as a melting pot in emergence of chimeric microorganisms. *Proc. Natl. Acad. Sci. USA* **106**, 21848-21853, https://doi.org/10.1073/pnas.0911354106 (2009).

530 26

531 Piskurek, O. & Okada, N. Poxviruses as possible vectors for horizontal transfer of

532 retroposons from reptiles to mammals. *Proc. Natl. Acad. Sci. USA* **104**, 12046-12051

533 https://doi.org/10.1073/pnas.0700531104 (2007).

534

535 27

536 Smit, AFA, Hubley, R. & Green, P. *RepeatMasker Open-4.0*. 2013-2015,

537 http://www.repeatmasker.org.

538

539 **Method-only references**

540 28

541 Luo, R. *et al.* SOAPdenovo2: an empirically improved memory-efficient short-read de

542 novo assembler. *GigaScience* **1**, 18, https://doi.org/10.1186/2047-217X-1-18 (2012).

543

544 29

545 Marçais, G. & Kingsford, C. A fast, lock-free approach for efficient parallel counting of

546 occurrences of k-mers. *Bioinformatics* **27**, 764–770,
547 https://doi.org/10.1093/bioinformatics/btr011 (2011).
548
549 30
550 Grabherr, M. G. et al. Full-length transcriptome assembly from RNA-Seq data without a
551 reference genome. *Nat. Biotechnol.* **29**, 644–652, https://doi.org/10.1038/nbt.1883
552 (2011).
553
554 31
555 Trapnell C., Pachter L. & Salzberg, S. L. TopHat: discovering splice junctions with
556 RNA-Seq. *Bioinformatics* **25**, 1105-1111, https://doi.org/10.1093/bioinformatics/btp120
557 (2009).
558
559 32
560 Trapnell, C. *et al.* Transcript assembly and quantification by RNA-Seq reveals
561 unannotated transcripts and isoform switching during cell differentiation. *Nat.*

562 *Biotechnol.* **28**, 511–515, https://doi.org/10.1038/nbt.1621 (2010).

563

564 33

565 Kent W. J. BLAT--the BLAST-like alignment tool. *Genome Res.* **12**, 656-664,

566 https://doi.org/10.1101/gr.229202 (2002).

567

568 34

569 Haas, B.J. *et al.* Improving the Arabidopsis genome annotation using maximal

570 transcript alignment assemblies. *Nucleic Acids Res.* **31**, 5654-5666,

571 https://doi.org/10.1093/nar/gkg770 (2003).

572

573 35

574 Bao, W., Kojima, K. K., & Kohany, O. Repbase Update, a database of repetitive

575 elements in eukaryotic genomes. *Mob. DNA* **6**, 11,

576 https://doi.org/10.1186/s13100-015-0041-9 (2015).

577

578 36

579 Camacho C. *et al.* BLAST+: architecture and applications. *BMC Bioinformatics* **10**, 421,

580 https://doi.org/10.1186/1471-2105-10-421 (2009).

581

582 37

583 Haas, B.J. *et al.* De novo transcript sequence reconstruction from RNA-seq using the

584 Trinity platform for reference generation and analysis. *Nat. Protoc.* **8**, 1494-1512,

585 https://doi.org/10.1038/nprot.2013.084 (2013).

586

587 38

588 Stanke, M., Diekhans, M., Baertsch, R. & Haussler, D. Using native and syntenically

589 mapped cDNA alignments to improve de novo gene finding. *Bioinformatics* **24**, 637–

590 644, https://doi.org/10.1093/bioinformatics/btn013 (2008).

591

592 39

593 Slater, G. S. & Birney, E. Automated generation of heuristics for biological sequence

comparison. *BMC Bioinformatics* **6**, 31, https://doi.org/10.1186/1471-2105-6-31 (2005).

40

Simão, F. A., Waterhouse, R. M., Ioannidis, P., Kriventseva, E. V. & Zdobnov E. M. BUSCO: assessing genome assembly and annotation completeness with single-copy orthologs. *Bioinformatics* **31**, 3210-3212, https://doi.org/10.1093/bioinformatics/btv351 (2015).

41

David, L. *et al.* Database resources of the National Center for Biotechnology. *Nucleic Acids Res.* **31**, 28–33, https://doi.org/10.1093/nar/gkg033 (2003).

42

Jones, P. et al. InterProScan 5: genome-scale protein function classification. *Bioinformatics* **30**, 1236–1240, https://doi.org/10.1093/bioinformatics/btu031 (2014).

610 43

611 Beissbarth, T. & Speed, T. P. GOstat: Find statistically overrepresented Gene
612 Ontologies within a group of genes. *Bioinformatics* **20**, 1464-1465,
613 https://doi.org/10.1093/bioinformatics/bth088 (2004).

614

615 44

616 Moriya, Y., Itoh, M., Okuda, S., Yoshizawa, A., & Kanehisa, M. KAAS: an automatic
617 genome annotation and pathway reconstruction server. *Nucleic Acids Res.* **35**,
618 W182-W185, https://doi.org/10.1093/nar/gkm321 (2007).

619

620 45

621 Emms, D. M. & Kelly S. OrthoFinder: solving fundamental biases in whole genome
622 comparisons dramatically improves orthogroup inference accuracy. *Genome Biol.* **16**,
623 157, https://doi.org/10.1186/s13059-015-0721-2 (2015).

624

625 46

626 Marchler-Bauer, A. et al. CDD/SPARCLE: functional classification of proteins via
627 subfamily domain architectures. *Nucleic Acids Res.* **45**, D200-D203,
628 https://doi.org/10.1093/nar/gkw1129 (2017).

629

630 47

631 Edgar R. C. MUSCLE: multiple sequence alignment with high accuracy and high
632 throughput. *Nucleic Acids Res.* **32**, 1792-1797, https://doi.org/10.1093/nar/gkh340
633 (2004).

634

635 48

636 Katoh, K., Misawa, K., Kuma, K. & Miyata T. MAFFT: a novel method for rapid
637 multiple sequence alignment based on fast Fourier transform. *Nucleic Acids Res.* **30**,
638 3059-3066, https://doi.org/10.1093/nar/gkf436 (2002).

639

640 49

641 Tamura, K., Stecher, G., Peterson, D., Filipski, A. & Kumar, S. MEGA6: Molecular

642 Evolutionary Genetics Analysis Version 6.0. *Mol. Biol. Evol.* **30**, 2725-2729,
643 https://doi.org/10.1093/molbev/mst197 (2013).
644
645 50
646 Kumar, S., Stecher, G., & Tamura, K. (2016) MEGA7: Molecular Evolutionary
647 Genetics Analysis Version 7.0 for bigger datasets. Mol. Biol. Evol. 33, 1870-1874,
648 https://doi.org/10.1093/molbev/msw054 (2016).
649
650 51
651 Kumar, S., Stecher, G., Peterson, D. & Tamura, K. MEGA-CC: Computing Core of
652 Molecular Evolutionary Genetics Analysis Program for Automated and Iterative Data
653 Analysis. *Bioinformatics* **28**, 2685-2686, https://doi.org/10.1093/bioinformatics/bts507
654 (2012).
655
656 52
657 Nguyen, L.-T., Schmidt, H.A., von Haeseler, A. & Minh, B.Q. IQ-TREE: A fast and

658 effective stochastic algorithm for estimating maximum likelihood phylogenies. *Mol.*
659 *Biol. Evol.* **32**, 268-274, https://doi.org/10.1093/molbev/msu300 (2015).
660
661 53
662 Tamura, K, Tao, Q. & Kumar S. Theoretical Foundation of the RelTime Method for
663 Estimating Divergence Times from Variable Evolutionary Rates. *Mol. Biol. Evol.* **35**,
664 1770–1782, https://doi.org/10.1093/molbev/msy044 (2018).
665
666 54
667 Capella-Gutiérrez S., Silla-Martínez, J. M. & Gabaldón, T. trimAl: a tool for automated
668 alignment trimming in large-scale phylogenetic analyses. *Bioinformatics* **25**, 1972-1973,
669 https://doi.org/10.1093/bioinformatics/btp348 (2009).
670
671 55
672 Criscuolo, A. & Gribaldo, S. BMGE (Block Mapping and Gathering with Entropy): a
673 new software for selection of phylogenetic informative regions from multiple sequence

674 alignments. *BMC Evol. Biol.* **10**, 210, https://doi.org/10.1186/1471-2148-10-210 (2010).

675

676 56

677 Badger M. R., Hanson, D. & Price G. D. Evolution and diversity of CO2 concentrating

678 mechanisms in cyanobacteria. *Funct. Plant Biol.* **29**, 161–173,

679 https://doi.org/10.1071/PP01213 (2002).

680

681 57

682 Marin, B., Nowack, E. C., Glöckner, G. & Melkonian, M. The ancestor of the Paulinella

683 chromatophore obtained a carboxysomal operon by horizontal gene transfer from a

684 Nitrococcus-like gamma-proteobacterium. *BMC Evol. Biol.* **7**, 85,

685 https://doi.org/10.1186/1471-2148-7-85 (2007).

686

687 58

688 Nowack, E. C. *et al.* Gene transfers from diverse bacteria compensate for reductive

689 genome evolution in the chromatophore of Paulinella chromatophora. *Proc. Natl. Acad.*

Sci. USA **113**, 12214-12219, https://doi.org/10.1073/pnas.1608016113 (2016).

59

Nowack, E. C. et al. Endosymbiotic gene transfer and transcriptional regulation of transferred genes in Paulinella chromatophora. *Mol. Biol. Evol.* **28**, 407-422, https://doi.org/10.1093/molbev/msq209 (2011).

60

Lhee, D. *et al.* Diversity of the Photosynthetic Paulinella Species, with the Description of Paulinella micropora sp. nov. and the Chromatophore Genome Sequence for strain KR01. *Protist* **168**, 155–170, https://doi.org/10.1016/j.protis.2017.01.003 (2017).

Acknowledgements

We thank Dr. Terabayashi T. for his kind instructions in SEM analysis. Computations were partially performed on the NIG supercomputer at ROIS National

706 Institute of Genetics. This work was supported by JSPS KAKENNHI grants: 221S0002,
707 15K14554, 1 and 6K14788, and by a Grant-in-Aid for Scientific Research on
708 Innovative Areas 3308 of the Ministry of Education, Culture, Sports, Science and
709 Technology of Japan.

710

711 **Author contributions**

712 M. M. prepared the *P. micropora* MYN1 genome samples, identified the
713 putative virus sequence in the *P. micorpora* MYN1 genome and wrote the draft
714 manuscript. M. M. and A. K. performed the RNA sample preparation. Y. M., H. N., A.
715 T. and A. F. performed the genome sequencing, the genome assembly and the Iso-Seq
716 analysis. Y. S. performed the RNA-seq sequencing analysis. M. N. and K. I. cultured *P.*
717 *micorpora* MYN1. M. M., A. K., M. T., H. N., H. T., S. S., M. N. and K. I. annotated
718 the *P. micropora* MYN1 genome. M. M., T. N. and R. K. performed the phylogenetic
719 analysis. T. N., R. K. and Y. I. analysed the organelle (chromatophore, mitochondria)
720 genome. J. O. organized and managed the *P. micropora* MYN1 genome project and
721 finalized the manuscript. We thank the members of Comparative Genomics

722 Laboratory in National Institute of Genetics for technical and computational
723 assistance.

724

725 **Competing interests**

726 The authors declare no competing interests.

727

728 **Materials & Correspondence**

729 Junichi Obokata

730 Email: obokata@kpu.ac.jp

731 Tel/Fax: +81-75-703-5164

732 Graduate School of Life and Environmental Science,

733 Kyoto Prefectural University, Kyoto, 606-8522, Japan

734

735

736

737

738 **Figure Legends**

739 **Fig. 1. An overview of the *P. micropora* MYN1 draft genome. a,** A SEM image of *P.*

740 *micropora* MYN1. **b,** The statistics of the draft genome. **c,** The genome composition of

741 *P. micropora* MYN1 analysed by RepeatMasker[27]. **d,** Simple repeats are extraordinarily

742 rich in *P. micropora* MYN1 compared with other organisms.

743

744 **Fig. 2. *P. micropora* nuclear genes acquired by EGT/HGT. a, b,** A functional

745 classification of the *P. micropora* nuclear genes derived from cyanobacteria (EGT

746 candidates) (**a**), and those from other bacteria (HGT candidates) (**b**). **c, d,** The amino

747 acid sequence identity of EGT candidates against *P. micropora* MYN1 plastid genes (**c**)

748 and that of HGT candidates against bacterial genes of the NCBI nr database (**d**). **e, f,** An

749 estimation of the gene transfer age for EGT candidates (**e**) and HGT candidates (**f**). The

750 endosymbiosis initiation period is green-highlighted. The ages of gene transfer in (**e**)

751 and (**f**) were calculated based on the divergent time points (45.7–64.7 MYA) of two

752 *Paulinella* species; thus, a gene transfer age younger than 60 MYA (striped phase)

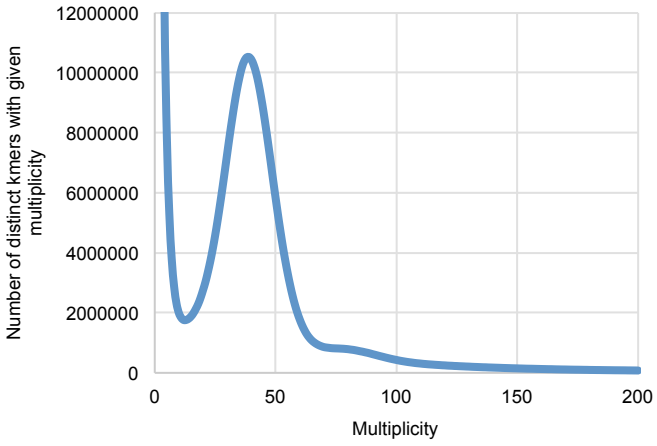
753 could not be estimated.

754

755 **Fig. 3. Putative DNA virus and mobile elements in *P. micropora* MYN1. a,** A
756 schematic view of DNA virus-like fragments and mobile elements in the *P. micropora*
757 draft genome (Scaffold 1104). The genomic regions were coloured according to the
758 sequence characteristics; putative dsDNA virus (pink), Polinton (light blue),
759 retrotransposon (brass yellow) and simple repeat-rich region (grey). The copy number
760 of the interspersed repeat elements was analysed by BLASTN against the
761 simple-repeat-masked *P. micropora* draft genome. **b,** ML phylogenetic tree of DNA
762 polymerases of viruses, eukaryotes and prokaryotes. **c,** Divergent time analysis of the
763 virus-type GPCR in *Paulinella*'s lineage. **d, e,** Divergent time analysis of DNA
764 polymerase genes of metazoa-type (**d**) and rhizarian-type (**e**) Polintons. Asterisks: the
765 branch point of *P. micropora* and *P. chromatophora* set at 45.7–64.7 MYA. Green
766 bands: initiation periods of endosymbiosis with cyanobacteria (93.6–141.4 MYA). *P.*
767 *micropora*; *Paulinella micropora* MYN1, *P. chromatophora*; *Paulinella*
768 *chromatophora* CCAC0185*, P. brassicae*; *Plasmodiophora brassicae*, *R. filosa*;
769 *Reticulomyxa filosa*, *S. purpurgus*; *Strongylocentrotus purpuratus*.

Fig. 4. Initial process of the endosymbiotic evolution of photosynthetic *Paulinella* species modeled from the *P. micropora* genomic data. 1) Predacious ancestors digested prey bacteria via phagocytosis with continuing low levels of HGT. **2)** The infection of large DNA virus triggered the massive HGT/EGT to promote the rapid endosymbiotic evolution. **3)** Acquiring photosynthetic competency shrunk the phagocytic activity to shut down the source of HGT/EGT. **4)** The photo-autotrophic *Paulinella* sp. contains one photosynthetic organelle per cell, hence, release of the organelle DNA hardly occurred without losing photosynthetic activity. In this final stage, virus-mediated gene transfer continued at trace level.

a



b

	Plastid (Chromatophore)	Mitochondria
Genome size (bp)	977,199	37,153
GC%	39.3	23.6
Protein coding gene	874	23
rRNA gene	3 (X2)	2
tRNA gene	42	20

c

Mapped cDNA-region (%)	No. of the mapped cDNAs	Percent (%) of the mapped cDNAs
>80	13747	99.7 (%)
>90	13606	98.7
>95	13279	96.3
100	10532	76.4

d

Species name	***P. micropora* MYN1**	***A. thaliana***	***P. brassicae***
Complete BUSCOs	388 (90%)	401 (93%)	392 (91%)
Complete Duplicated BUSCOs	139 (32%)	268 (62%)	95 (22%)
Fragmented BUSCOs	19 (4.4%)	10 (2.3%)	17 (3.9%)
Missing BUSCOs	22 (5.1%)	18 (4.1%)	20 (4.6%)

e

Biological process

GO ID	Description	p-value
GO:0015074	DNA integration	0
GO:0006259	DNA metabolic process	0
GO:0006260	DNA replication	0
GO:0006139	nucleobase, nucleoside, nucleotide and nucleic acid metabolic process	0
GO:0043283	biopolymer metabolic process	4.39E-65
GO:0043170	macromolecule metabolic process	6.18E-36
GO:0009186	deoxyribonucleoside diphosphate metabolic process	7.42E-21
GO:0009262	deoxyribonucleotide metabolic process	3.35E-17
GO:0009132	nucleoside diphosphate metabolic process	7.65E-17
GO:0000160	two-component signal transduction system (phosphorelay)	4.40E-15

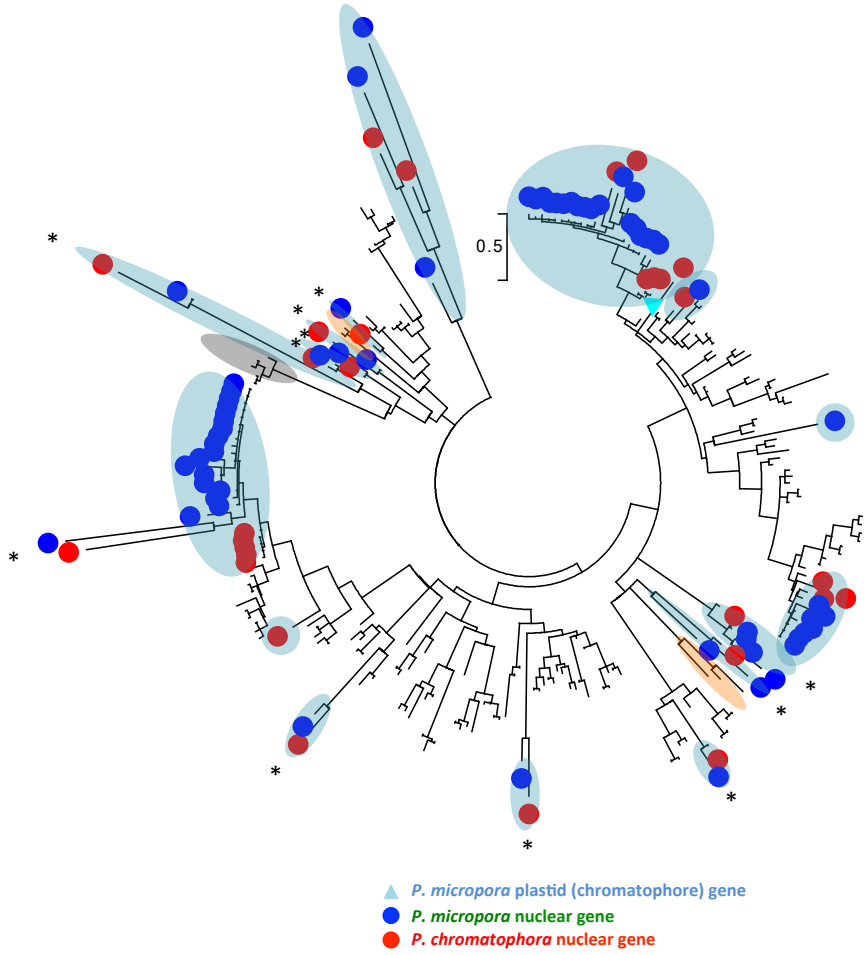
Cellular component

GO ID	Description	p-value
GO:0005578	proteinaceous extracellular matrix	6.52E-05
GO:0000785	chromatin	0.009764
GO:0000786	chromatin#nucleosome	0.009764

Molecular function

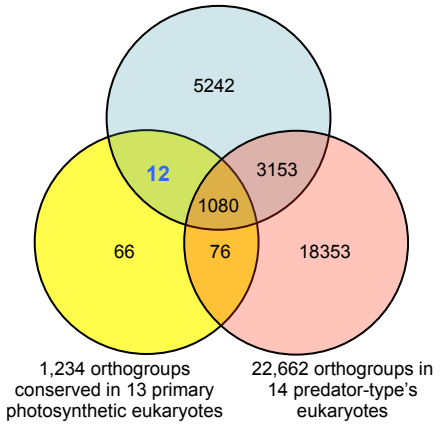
GO ID	Description	p-value
GO:0003688	DNA replication origin binding	2.85E-77
GO:0043565	sequence-specific DNA binding	2.39E-59
GO:0008270	zinc ion binding	1.73E-41
GO:0046914	transition metal ion binding	8.56E-36
GO:0004930	G-protein coupled receptor activity	3.70E-22
GO:0003899	DNA-directed RNA polymerase activity	1.67E-20
GO:0004888	transmembrane receptor activity	1.10E-17
GO:0016775	phosphotransferase activity, nitrogenous group as acceptor	3.57E-16
GO:0004673	protein histidine kinase activity	3.57E-16
GO:0000155	two-component sensor activity	3.57E-16

Extended Data Fig. 1. Information of the *P. micropora* MYN1 genome. a, Estimation of the *P. micropora* MYN1 genome by K-mer frequency analysis. Single peak at 39 of the multiplicity are detected with 31-mer, utilizing 52,592,411,100 b from Illumina 500b pair-end reads. From the peak value and the used reads length, 1.35 Gb genome size was estimated. **b,** Summary of the *P. micropora* MYN1 organelle genome. **c,** Validation of the genome assembly by mapping of the sequences of the isoform sequencing (Iso-Seq) transcripts. 13787 non-redundant Iso-Seq sequences of the intron-containing genes, either hitting protein sequences of the Swiss-Prot database by BLASTX search (e-value ≤ $1e^{-60}$) or containing long ORFs (≥ 300 amino acids), were mapped on the draft genome. **d,** Assessment of the genome assembly using 429 BUSCO v. 1 (Benchmarking Universal Single-Copy Orthologs) genes. In comparison with other eukaryote genome assemblies, the BUSCO values of a photosynthetic organism (*Arabidopsis thaliana*) and that of the well-assembled genome of a rhizarian organism (*Plasmodiophora brassicae*) are shown. **e,** The top 10 GO-terms that are significantly overrepresented in the *P. micropora* MYN1 genome compared with other rhizarian organisms (*Bigelowiella natans*, *Plasmodiophora brassicae*, *Reticulomyxa filosa*). Fisher's exact test p-values corrected with false discovery rate (Benjamini) are represented.



Extended Data Fig. 2. A ML phylogenetic tree of Hlips of *P. micropora* MYN1 and *P. chromatophora.* Hlips of cyanobacteria, photosynthetic eukaryotes and cyanophages are used as a reference for operational taxonomy units. Sixty-four *P. micropora* Hlip genes were subjected to phylogenetic analysis and grouped according to the clade. The redundant paralogs of identical sequences were removed. Asterisks: *Paulinella* ortholog-pair supported by a bootstrap value >70. Blue and red circle: nuclear encoded Hlip of *P. micropora* and *P. chromatophora*. Light-blue triangle: *P. micropora* plastid (chromatophore) Hlip. Phylogenetic branch of the *Paulinella* gene (light blue), virus (grey) and eukaryote Hlip-like gene (orange) are highlighted.

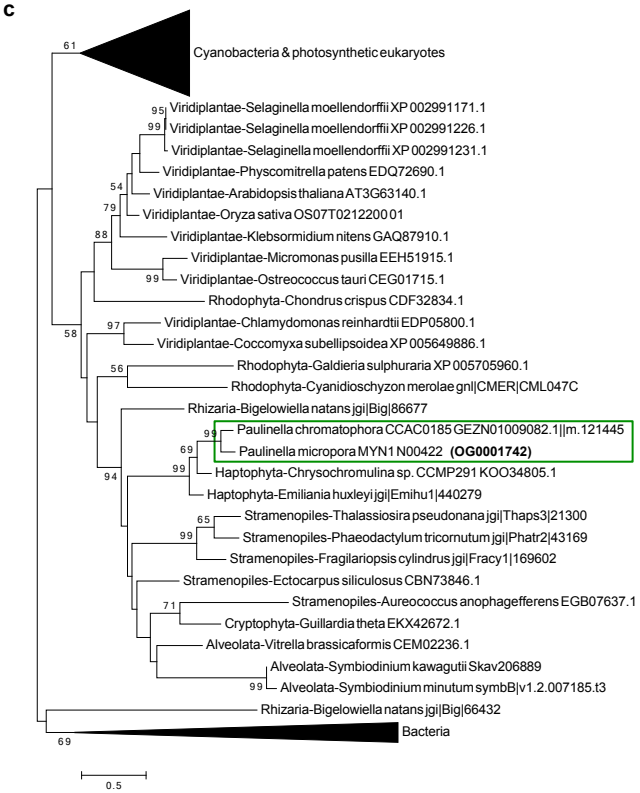
a



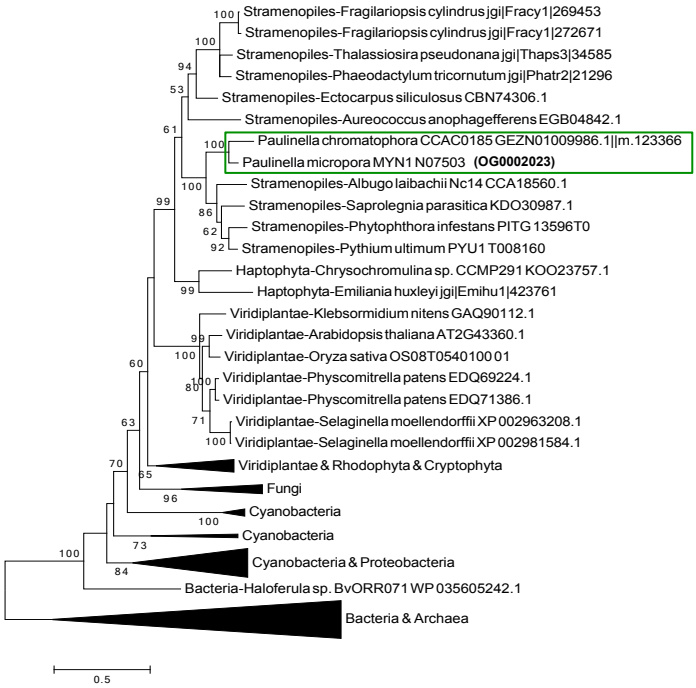
b

Orthogroup ID	Function	No. of *P. micropora* genes	Cellular localization of the orthologs in *A. thaliana*	Estimated origin
OG0000217	Chlorophyll A-B binding family protein (High light inducible protein)	81	Plastid	Cyanobacteria or Photosynthetic-eukaryote
OG0000633	Probable plastid-lipid-associated protein	4	Plastid	Cyanobacteria or Photosynthetic-eukaryote
OG0000868	Zeta-carotene desaturase	1	Plastid	Bacteria
OG0001101	Acetylglutamate kinase	1	Plastid	Bacteria
OG0001187	Arogenate dehydratase/prephenate dehydratase	1	Plastid	Unknown
OG0001403	Unknown	3	unknown	Cyanobacteria
OG0001742	Plastid stem-loop binding protein of 41kDa	1	Plastid	Haptophyta
OG0001936	SOUL heme-binding family protein	2	Plastid, golgi, vacuole	Bacteria and eukaryote
OG0002023	Biotin synthase	1	Mitochondoria	Stramenopiles
OG0003327	Unknown	1	Plastid	Cyanobacteria or Photosynthetic-eukaryote
OG0004091	Unknown	1	Plastid	Photosynthetic-eukaryote
OG0005438	Probable glutamyl endopeptidase,	1	Plastid	Rhizaria

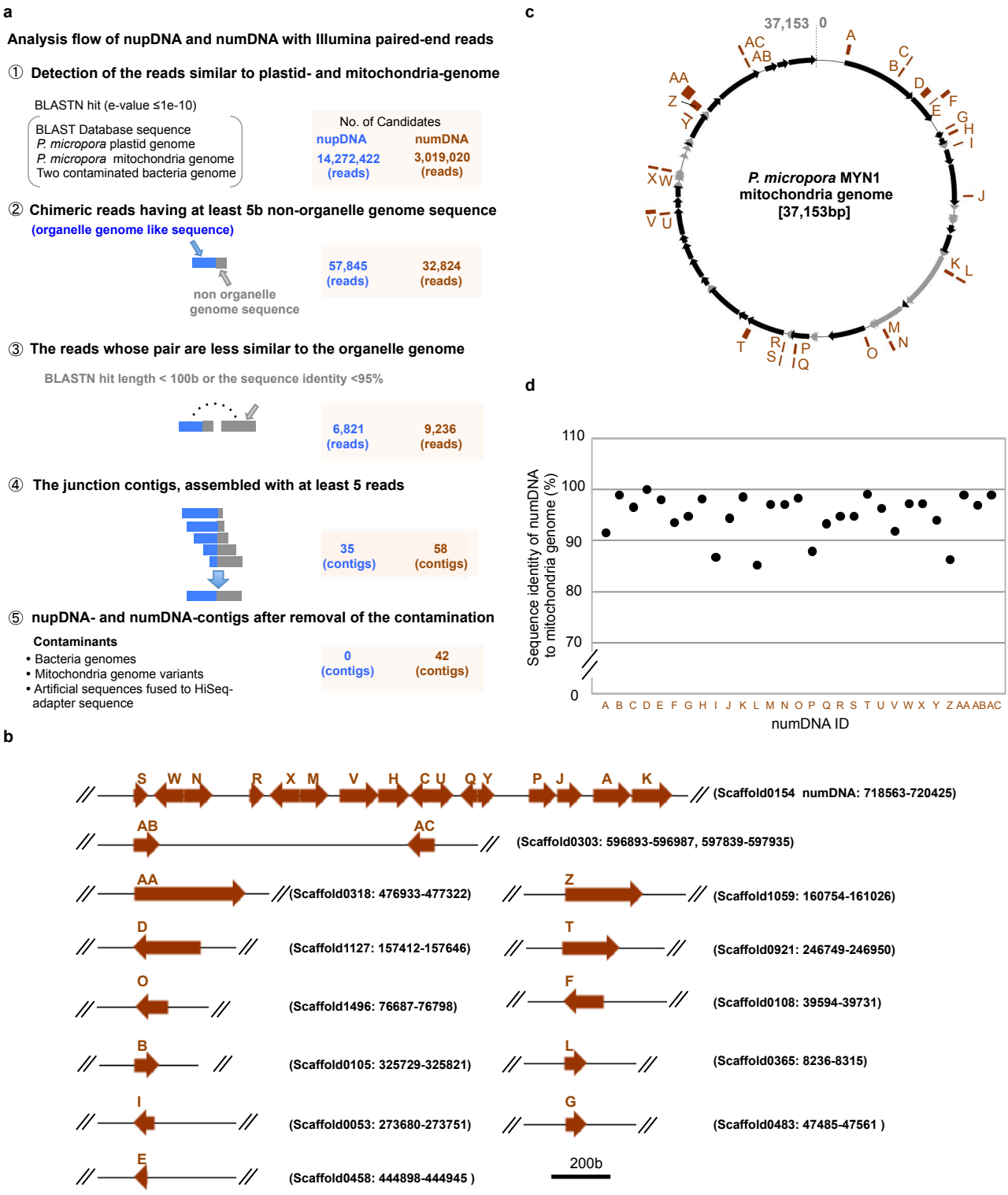
c



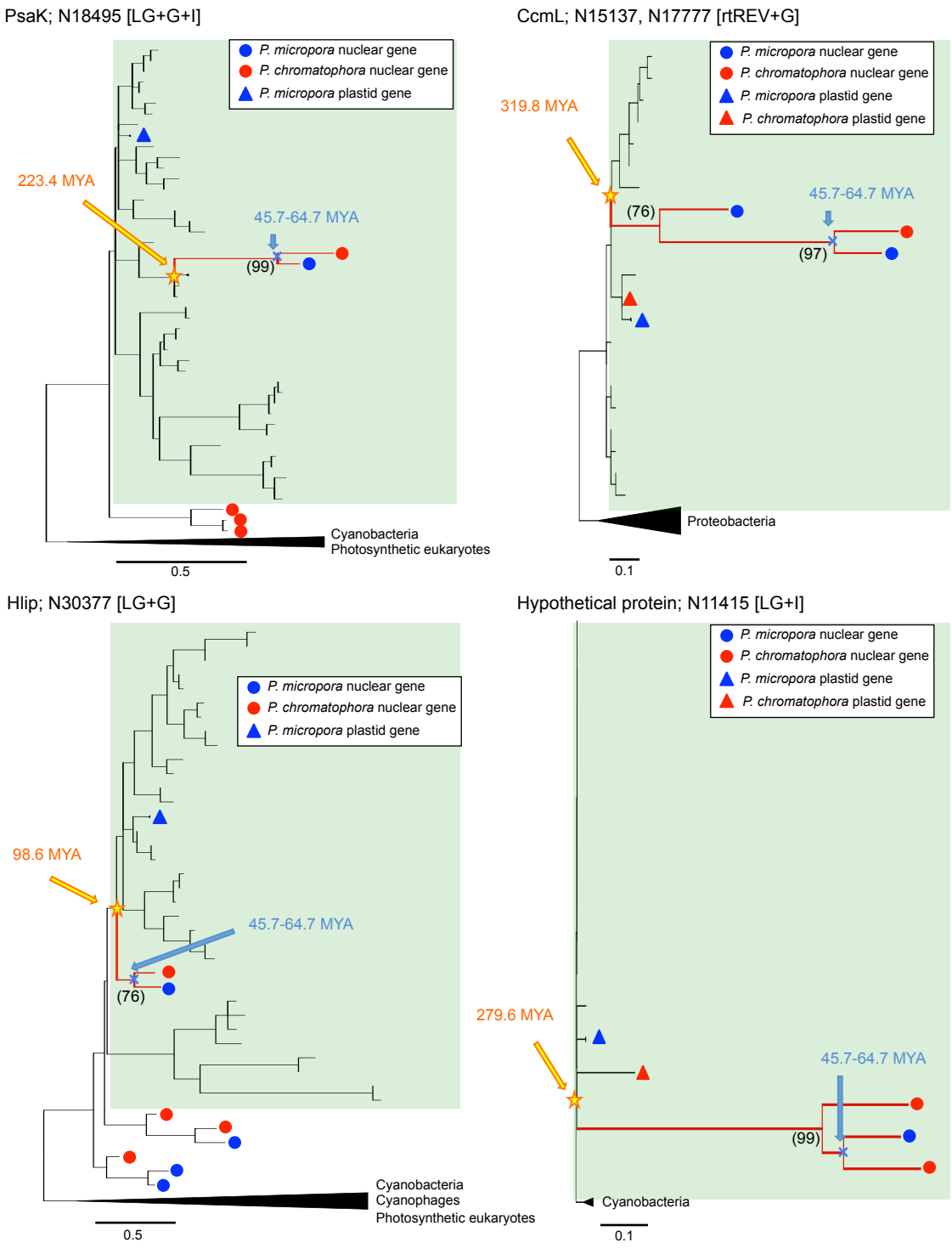
d



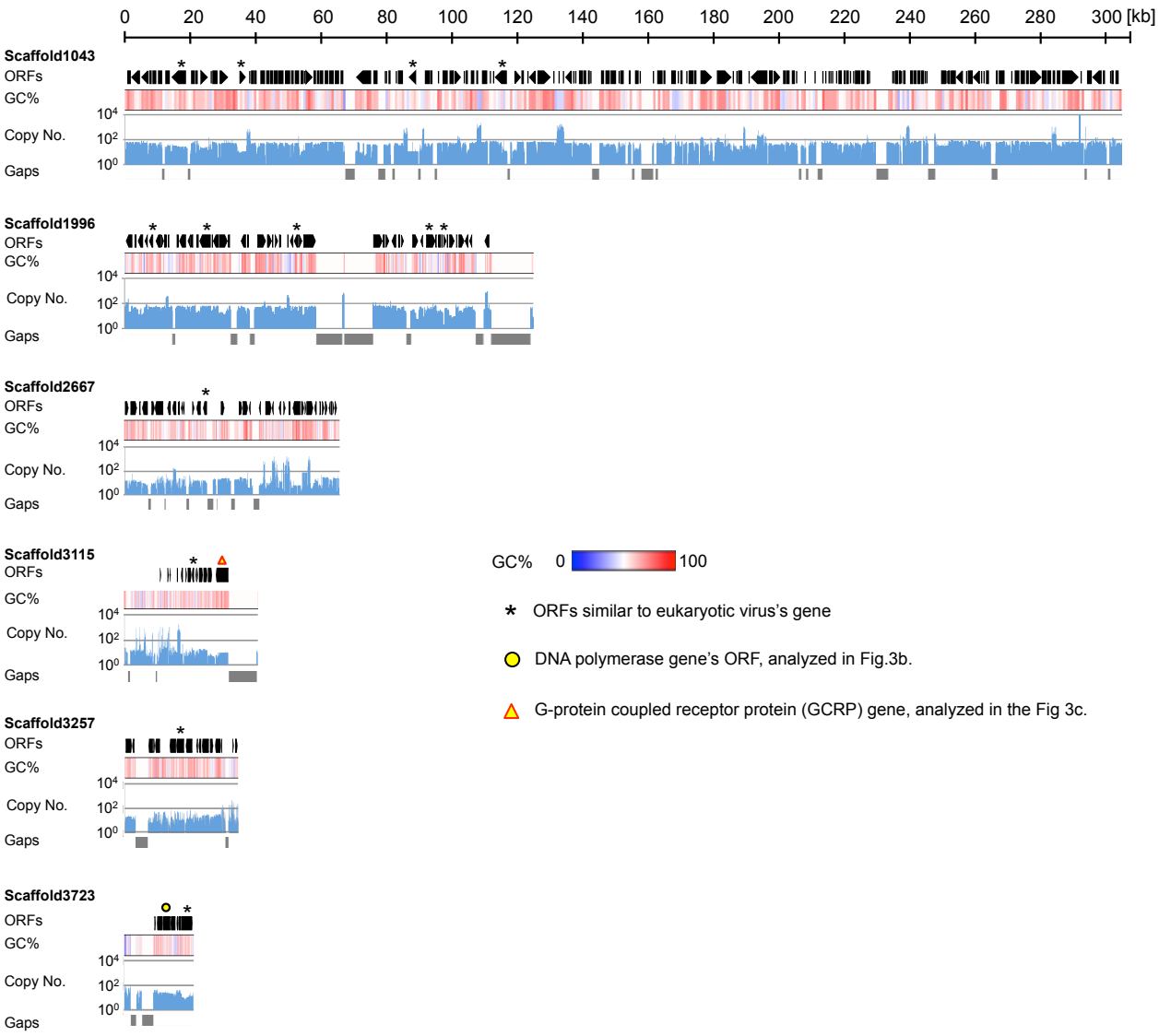
Extended Data Fig. 3. Comparison of the orthogroups of *P. micropora*, primary photosynthetic eukaryotes and predator-type eukaryotes. a, Venn diagram of *P. micriopora* orthogroups with the predator-type eukaryote orthogroups and the conserved orthogroups in primary photosynthetic eukaryotes. Orthogroups were detected by Orthofinder from the gene sets of *P. micropora* MYN1, 14 predator eukaryotes (*Acanthamoeba castellanii*, *Dictyostelium discoideum*, *Entamoeba histolytica HM-1*, *Bodo saltans*, *Naegleria gruberi*, *Caenorhabditis_elegans*, *Drosophila melanogaster*, *Monosiga brevicollis MX1*, *Oxytricha trifallax, Paramecium tetraurelia*, *Stylonychia lemnae*, *Tetrahymena thermophila*, *Reticulomyxa filosa*, *Thecamonas trahens ATCC50062*) and 13 photosynthetic eukaryotes (*Arabidopsis thaliana*, *Chlamydomonas reinhardtii*, *Coccomyxa subellipsoidea C-169*, *Klebsormidium nitens*, *Micromonas pusilla CCMP1545*, *Oryza sativa*, *Ostreococcus tauri*, *Physcomitrella patens*, *Selaginella moellendorffii*, *Chondrus crispus*, *Cyanidioschyzon merolae*, *Galdieria sulphuraria*, *Cyanophora paradoxa*). **b,** Annotations of 12 orthogroups conserved in primary photosynthetic eukaryotes, but not in predator eukaryotes. The functional annotation and the cellular localization were based on UniprotKB information of *Arabidopsis thaliana* orthologs, and manual annotations are represented in parenthesis. The estimated origins were based on the ML phylogenetic analysis. Genes involved in light acclimation (cyan), nutrient auxotrophy (yellow) and organelle gene expression (magenta) are highlighted. **c** and **d,** ML phylogenetic trees of orthogroup genes acquired by HGT from other eukaryotes; Haptophyta (**c**, OG0001742) and Stramenopiles (**d**, OG0002023). The phylogenetic analysis of **c** and **d** were performed using a LG+G (**c**) and a LG+G+I model (**d**), respectively. Photosynthetic *Paulinella* species are boxed.



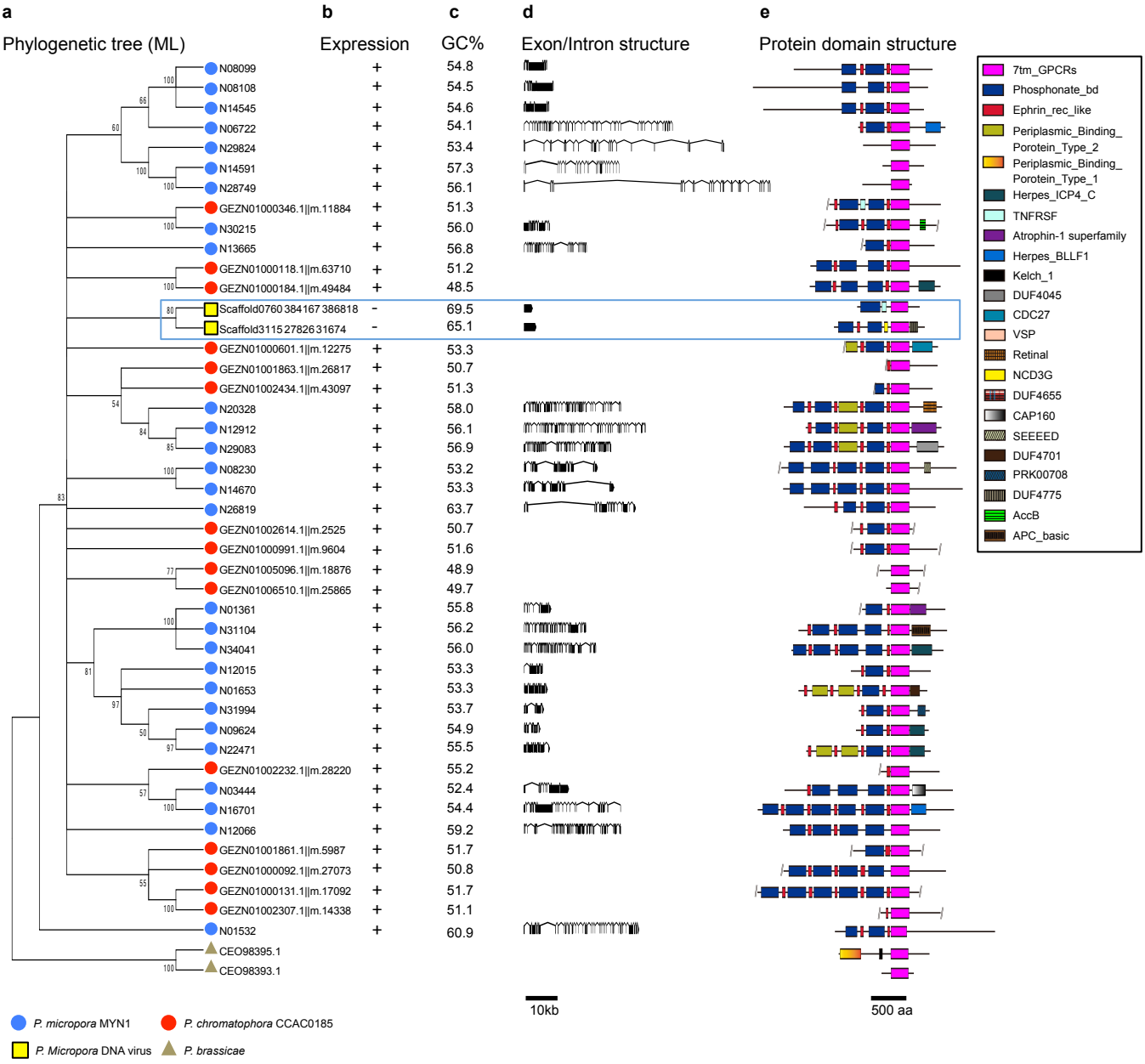
Extended Data Fig. 4. Analysis of nuclear-localized plastid DNA (nupDNA) and mitochondria DNA (numDNA) in *P. micropora*. **a,** Analysis of the junction sequences of nupDNA and numDNA using Illumina raw-reads sequences. 902,121,079 quality-trimmed HiSeq paired-end sequence reads (insert size: 300 b, 500 b) were analysed. **b,** numDNA sequence structures in the *P. micropora* draft genome. **c**, Distribution of numDNA sequences in mitochondrial genome positions. **d,** Nucleotide percent identity of numDNA compared with the mitochondria genome sequence. NumDNA directions are represented by right and left arrows which denote clockwise- and anti-clockwise directions of the mitochondria genome sequence (**c**), respectively.



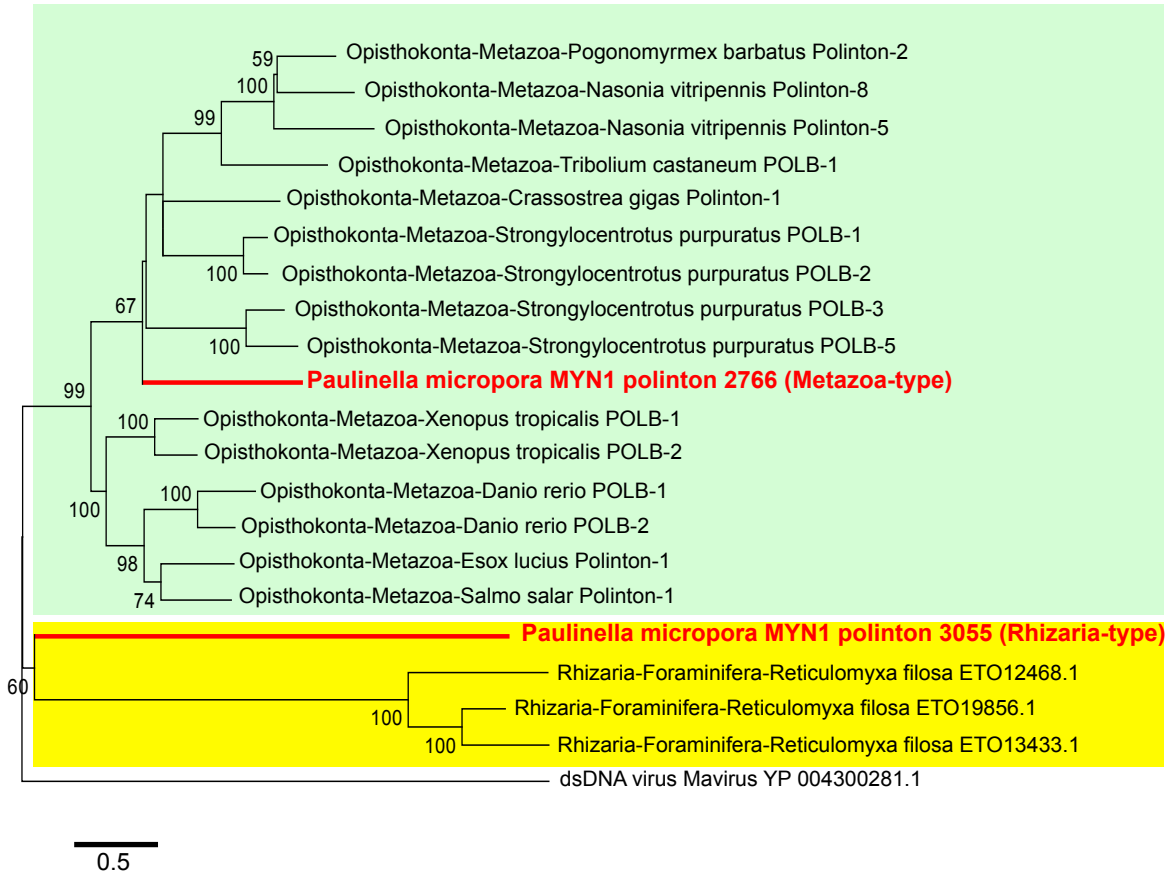
Extended Data Fig. 5. ML phylogenetic trees of four EGT candidates whose counterpart orthologs are found in the plastid (chromatophore) genome of *P. micropora*. The clades of the *Paulinella* plastid and cyanobacteria are highlighted in green. Blue circle: *P. micropora* nuclear gene, red circle: *P. chromatophora* nuclear gene, blue triangle: *P. micropora* plastid gene, red triangle: *P. chromatophora* plastid gene, unmarked: cyanobacterium gene. The branch of *P. micropora* and *P. chromatophora* nuclear genes supported by high bootstraps (numbers in the parenthesis) is represented as a red line. The divergence time of *Paulinella* nuclear genes from the plastid- or other cyanobacterial-genes (yellow stars) were estimated by RelTime methods of MEGA6 using the divergent time of *P. micropora* and *P. chromatophora* (45.7–64.7 MYA) (blue cross). Psak: Photosystem I subunit K, CcmL: CO_2 concentrating mechanism protein, Hlip: High light inducible protein. Brackets mean the substitution model used in the phylogenetic analysis. Trees with species names are available at the repository (https://figshare.com/s/a665678c48d0af073894).



Extended Data Fig. 6. Putative DNA virus fragments detected in the *P. micropora* draft genome. ORF structures, GC%, copy number and sequence gaps are represented as described in the legend to Fig. 3.



Extended Data Fig. 7. Characteristics of virus-type GPCRs of *P. micropora* and *P. chromatophora*. **a,** A ML phylogenetic tree of seven transmembrane domains of GPCRs. GPCRs in *P. micropora, P. chromatophora, P. brassicae* (CEO98393.1, CEO98395.1), and those detected in DNA viral fragments were analysed using a LG+G+F model. Branches with bootstrap values <50 are condensed. **b,** Existence of the transcript. **c,** GC% of the coding sequence of GPCR genes. **d,** Exon/intron structures of the genes. **e,** Protein domain structures. Protein domains were detected by CD search[48]. GPCRs in putative DNA viruses are boxed with a blue line.



Extended Data Fig. 8. ML phylogenetic tree of DNA polymerases of Polintons. a, DNA polymerase sequences of *P. micropora* Polintons (No. 2766 and No. 3055), *R. filosa'* Polintons (Genbank, ETO12468.1, ETO19856.1, ETO13433.1), metazoan Polintons in Repbase [37] and Mavirus (Genbank, YP 004300281.1) were analysed with a LG+G+I model. The metazoan and rhizarian groups are highlighted in green and yellow, respectively.

786 **Extended Data legends**

787 **Extended Data Fig. 1. Information of the *P. micropora* MYN1 genome. a,**
788 Estimation of the *P. micropora* MYN1 genome size by K-mer frequency analysis.
789 Single peak at 39 of the multiplicity are detected with 31-mer, utilizing 52,592,411,100
790 b from Illumina 500b pair-end reads. From the peak value and the used reads length,
791 1.35 Gb genome size was estimated. **b,** Summary of the *P. micropora* MYN1 organelle
792 genome. **c,** Validation of the genome assembly by mapping of the sequences of the
793 isoform sequencing (Iso-Seq) transcripts. 13787 non-redundant Iso-Seq sequences of
794 the intron-containing genes, either hitting protein sequences of the Swiss-Prot database
795 by BLASTX search (e-value ≤ $1e^{-60}$) or containing long ORFs (≥ 300 amino acids),
796 were mapped on the draft genome. **d,** Assessment of the genome assembly using 429
797 BUSCO v. 1 (Benchmarking Universal Single-Copy Orthologs) genes. In comparison
798 with other eukaryote genome assemblies, the BUSCO values of a photosynthetic
799 organism (*Arabidopsis thaliana*) and that of the well-assembled genome of a rhizarian
800 organism (*Plasmodiophora brassicae*) are shown. **e,** The top 10 GO-terms that are
801 significantly overrepresented in the *P. micropora* MYN1 genome compared with other

802 rhizarian organisms (*Bigelowiella natans*, *Plasmodiophora brassicae*, *Reticulomyxa*
803 *filosa*). Fisher's exact test p-values corrected with false discovery rate (Benjamini) are
804 represented.
805
806 **Extended Data Fig. 2. A ML phylogenetic tree of Hlips of *P. micropora* MYN1 and**
807 ***P. chromatophora.*** Hlips of cyanobacteria, photosynthetic eukaryotes and cyanophages
808 are used as a reference for operational taxonomy units. Sixty-four *P. micropora* Hlip
809 genes were subjected to phylogenetic analysis and grouped according to the clade. The
810 redundant paralogs of identical sequences were removed. Asterisks: *Paulinella*
811 ortholog-pair supported by a bootstrap value >70. Blue and red circle: nuclear encoded
812 Hlip of *P. micropora* and *P. chromatophora*. Light-blue triangle: *P. micropora* plastid
813 (chromatophore) Hlip. Phylogenetic branch of the *Paulinella* gene (light blue), virus
814 (grey) and eukaryote Hlip-like gene (orange) are highlighted.
815
816 **Extended Data Fig. 3. Comparison of the orthogroups of *P. micropora,* primary**
817 **photosynthetic eukaryotes and predator-type eukaryotes. a,** Venn diagram of *P.*

818 *micriopora* orthogroups with the predator-type eukaryote orthogroups and the
819 conserved orthogroups in primary photosynthetic eukaryotes. Orthogroups were
820 detected by Orthofinder from the gene sets of *P. micropora* MYN1, 14 predator
821 eukaryotes (*Acanthamoeba castellanii*, *Dictyostelium discoideum*, *Entamoeba*
822 *histolytica HM-1*, *Bodo saltans*, *Naegleria gruberi*, *Caenorhabditis_elegans*,
823 *Drosophila melanogaster*, *Monosiga brevicollis MX1*, *Oxytricha trifallax, Paramecium*
824 *tetraurelia*, *Stylonychia lemnae*, *Tetrahymena thermophila*, *Reticulomyxa filosa*,
825 *Thecamonas trahens ATCC50062*) and 13 photosynthetic eukaryotes (*Arabidopsis*
826 *thaliana*, *Chlamydomonas reinhardtii*, *Coccomyxa subellipsoidea C-169*,
827 *Klebsormidium nitens*, *Micromonas pusilla CCMP1545*, *Oryza sativa*, *Ostreococcus*
828 *tauri*, *Physcomitrella patens*, *Selaginella moellendorffii*, *Chondrus crispus*,
829 *Cyanidioschyzon merolae*, *Galdieria sulphuraria*, *Cyanophora paradoxa*). **b,**
830 Annotations of 12 orthogroups conserved in primary photosynthetic eukaryotes, but not
831 in predator eukaryotes. The functional annotation and the cellular localization were
832 based on UniprotKB information of *Arabidopsis thaliana* orthologs, and manual
833 annotations are represented in parenthesis. The estimated origins were based on the ML

834 phylogenetic analysis. Genes involved in light acclimation (cyan), nutrient auxotrophy
835 (yellow) and organelle gene expression (magenta) are highlighted. **c** and **d,** ML
836 phylogenetic trees of orthogroup genes acquired by HGT from other eukaryotes;
837 Haptophyta (**c**, OG0001742) and Stramenopiles (**d**, OG0002023). The phylogenetic
838 analysis of **c** and **d** were performed using a LG+G (**c**) and a LG+G+I model (**d**),
839 respectively. Photosynthetic *Paulinella* species are boxed.
840
841 **Extended Data Fig. 4. Analysis of nuclear-localized plastid DNA (nupDNA) and**
842 **mitochondria DNA (numDNA) in *P. micropora.* a,** Analysis of the junction sequences
843 of nupDNA and numDNA using Illumina raw-reads sequences. 902,121,079
844 quality-trimmed HiSeq paired-end sequence reads (insert size: 300 b, 500 b) were
845 analysed. **b,** numDNA sequence structures in the *P. micropora* draft genome. **c**,
846 Distribution of numDNA sequences in mitochondrial genome positions. **d,** Nucleotide
847 percent identity of numDNA compared with the mitochondria genome sequence.
848 NumDNA directions are represented by right and left arrows which denote clockwise-
849 and anti-clockwise directions of the mitochondria genome sequence (**c**), respectively.

850

851 **Extended Data Fig. 5. ML phylogenetic trees of four EGT candidates whose**
852 **counterpart orthologs are found in the plastid (chromatophore) genome of *P.***
853 ***micropora.*** The clades of the *Paulinella* plastid and cyanobacteria are highlighted in
854 green. Blue circle: *P. micropora* nuclear gene, red circle: *P. chromatophora* nuclear
855 gene, blue triangle: *P. micropora* plastid gene, red triangle: *P. chromatophora* plastid
856 gene, unmarked: cyanobacterium gene. The branch of *P. micropora* and *P.*
857 *chromatophora* nuclear genes supported by high bootstraps (numbers in the parenthesis)
858 is represented as a red line. The divergence time of *Paulinella* nuclear genes from the
859 plastid- or other cyanobacterial-genes (yellow stars) were estimated by RelTime
860 methods of MEGA6 using the divergent time of *P. micropora* and *P. chromatophora*
861 (45.7–64.7 MYA) (blue cross). Psak: Photosystem I subunit K, CcmL: CO_2
862 concentrating mechanism protein, Hlip: High light inducible protein. Brackets mean the
863 substitution model used in the phylogenetic analysis. Trees with species names are
864 available at the repository (https://figshare.com/s/a665678c48d0af073894).

865

866 **Extended Data Fig. 6. Putative DNA virus fragments detected in the *P. micropora***
867 **draft genome.** ORF structures, GC%, copy number and sequence gaps are represented
868 as described in the legend to Fig. 3.

869

870 **Extended Data Fig. 7. Characteristics of virus-type GPCRs of *P. micropora* and *P.***
871 ***chromatophora.*** **a,** A ML phylogenetic tree of seven transmembrane domains of
872 GPCRs. GPCRs in *P. micropora, P. chromatophora, P. brassicae* (CEO98393.1,
873 CEO98395.1), and those detected in DNA viral fragments were analysed using a
874 LG+G+F model. Branches with bootstrap values <50 are condensed. **b,** Existence of the
875 transcript. **c,** GC% of the coding sequence of GPCR genes. **d,** Exon/intron structures of
876 the genes. **e,** Protein domain structures. Protein domains were detected by CD search[48].
877 GPCRs in putative DNA viruses are boxed with a blue line.

878

879 **Extended Data Fig. 8. ML phylogenetic tree of DNA polymerases of Polintons. a,**
880 DNA polymerase sequences of *P. micropora* Polintons (No. 2766 and No. 3055), *R.*
881 *filosa'* Polintons (Genbank, ETO12468.1, ETO19856.1, ETO13433.1), metazoan

Polintons in Repbase[37] and Mavirus (Genbank, YP 004300281.1) were analysed with a LG+G+I model. The metazoan and rhizarian groups are highlighted in green and yellow, respectively.

Supplementary information

Supplementary Table 1. Summary of the raw sequence data of the *P. micropora* genome.

Supplementary Table 2. Annotation and categorization of the *P. micropora* RepeatModeller sequences. *The categorization is based on the sequence similarities with the manually curated repeat sequences in Supplementary Table 3 by BLASTX search (e-value < $1e^{-5}$).

Supplementary Table 3. Annotation of the repeat elements manually identified from the *P. micropora* draft genome. *The copy number of the repeat elements was

898 estimated by BLASTN search against the *P. micropora* genome. Redundant BLASTN
899 hits at the same genome locus were manually removed.

900

901 **Supplementary Table 4. *P. micropora* MYN1 gene list.**

902

903 **Supplementary Table 5. GO-terms over- and under-represented in the *P.***
904 ***micropora* MYN1 genome compared with the genome of other rhizarian organisms**
905 **(*B. natans, P. brassicae and R.filosa*).** Significantly enriched GO-terms with Fisher's
906 exact test p-value less than 0.01 are represented.

907

908 **Supplementary Table 6. EGT and HGT candidates in *P. micropora* MYN1.** Genes
909 satisfying at least one of the following criteria were considered as EGT and HGT
910 candidates. 1) No hits to eukaryote genes of the NCBI nr database by BLAST analysis*
911 2) EGT and HGT are supported by ML phylogenetic analysis with a high bootstrap
912 value (≥95) except when the phylogenetically available protein alignment sequences
913 were short (< 100 amino acids)** 3) *P. micropora* genes were embedded in the clade of

914 photosynthetic organisms in the phylogenetic tree. * BLASTP top 1000 hits (NCBI nr,
915 e-value < $1e^{-10}$) were classified. A: Archaea, B: Bacteria, E: Eukaryotes, V: Viruses, O:
916 Others, U: Unknown. ** We lowered the threshold of the bootstrap value to 70 when
917 the alignment sequence positions available for the phylogenetic analysis were less than
918 100 amino acids.
919
920 **Supplementary Table 7. Detection of P. *micropora* Polintons by tBLASTn search**
921 **using DNA polymerase domain sequences.** A tBLASTn search was performed against
922 the *P. micropora* draft genome (e-value < $1e^{-10}$). The draft genome sequences and the
923 query sequences are available at the repository
924 (https://figshare.com/s/a665678c48d0af073894).
925
926 **Supplementary Table 8. Accession numbers of P. micropora MYN1 genome**
927 **sequences.**
928
929 **Supplementary Table 9. Parameters of the ML phylogenetic analysis by MEGA6.**

930

931 **Supplementary Table 10. Sequence data used in this study.**

932

933

934

935

936

937

938

939

940

941

942

943

944

945